Seasonal variations in the production of singlet oxygen and organic triplet excited states in aqueous PM$_{2.5}$ in Hong Kong, South China

Yuting Lyu[1], Yin Hau Lam[1], Yitao Li[1], Nadine Borduas-Dedekind[2], and Theodora Nah[1,3]

[1]School of Energy and Environment, City University of Hong Kong, Hong Kong SAR, China
[2]Department of Chemistry, University of British Columbia, Vancouver V6T 1Z1, Canada
[3]State Key Laboratory of Marine Pollution, City University of Hong Kong, Hong Kong SAR, China

Correspondence: Theodora Nah (theodora.nah@cityu.edu.hk)

Abstract. Photooxidants drive many atmospheric chemical processes. The photoexcitation of light-absorbing organic compounds (i.e., brown carbon (BrC)) in atmospheric waters can lead to the generation of reactive organic triplet excited states ($^3C^*$), which can undergo further reactions to produce other photooxidants such as singlet oxygen ($^1O_2^*$). To determine the importance of these aqueous photooxidants in SOA formation and transformation, we must know their steady-state concentrations and quantum yields. However, there has been limited measurements of aqueous $^3C^*$ and $^1O_2^*$ in atmospheric samples outside of North America and Europe. In this work, we report the first measurements of the steady-state concentrations and quantum yields of $^3C^*$ and $^1O_2^*$ produced in aerosols in South China. We quantified the production of $^3C^*$ and $^1O_2^*$ in illuminated aqueous extracts of PM$_{2.5}$ collected in different seasons at two urban sites and one coastal semi-rural site during a year-round study conducted in Hong Kong, South China. The mass absorption coefficients at 300 nm for BrC in the aqueous PM$_{2.5}$ extracts ranged from 0.49 to 2.01 m^2 g-C^{-1} for the three sites. Both $^1O_2^*$ and $^3C^*$ were produced year-round. The steady-state concentrations of $^1O_2^*$ ([$^1O_2^*$]$_{ss}$) in the illuminated aqueous extracts ranged from 1.56×10^{-14} to 1.35×10^{-12} M, with a study average of $(4.02 \pm 3.52) \times 10^{-13}$ M. Nearly two orders of magnitude lower than [$^1O_2^*$]$_{ss}$, the steady-state concentrations of $^3C^*$ ([$^3C^*$]$_{ss}$) ranged from 2.93×10^{-16} to 8.08×10^{-14} M, with a study average of $(1.09 \pm 1.39) \times 10^{-14}$ M. The quantum yields of $^1O_2^*$ and $^3C^*$ also spanned wide ranges across samples, with a range of 1.19 to 13.74 % and an average of (5.19 ± 2.63) % for $^1O_2^*$, and a range of 0.05 to 3.24 % and an average of (0.56 ± 0.66) % for $^3C^*$. The [$^1O_2^*$]$_{ss}$ and [$^3C^*$]$_{ss}$ correlated with the concentration and absorbance of BrC, thus implying that the amount of BrC drives the steady-state concentrations of these photooxidants. The locations (urban vs. semi-rural) did not have a significant effect on [$^3C^*$]$_{ss}$ and [$^1O_2^*$]$_{ss}$, which indicated that BrC from local sources did not have a significant influence on the year-round $^3C^*$ and $^1O_2^*$ production. $^3C^*$ and $^1O_2^*$ production were found to be the highest in winter and the lowest in summer for all three sites. The observed seasonal trends of $^1O_2^*$ and $^3C^*$ production could be attributed to the seasonal variations in long-range air mass transport. Our analysis highlighted the key role that regional sources play in influencing the composition and concentrations of water-soluble BrC in winter PM$_{2.5}$ in Hong Kong, which contributed to their highest $^3C^*$ and $^1O_2^*$ production. The current results will be useful for modeling seasonal aqueous organic aerosol photochemistry in the South China region.

1 Introduction

Atmospheric aqueous phases (e.g., aqueous aerosol, cloud water, fog droplets) serve as important media for chemical reactions of organic compounds. Many of the chemical transformations in atmospheric aqueous phases are driven by photochemically generated oxidants, particularly triplet excited states of organic matter ($^3C^*$), singlet state oxygen ($^1O_2^*$), and hydroxyl radicals ($\cdot OH$). Light absorbing organic compounds, commonly known as brown carbon (BrC), serve as key precursors for the formation of photooxidants in atmospheric aqueous phases (Laskin et al., 2015; Hems et al., 2021).

Upon the absorption of sunlight, some BrC chromophores (e.g., aromatic carbonyls) can be promoted from their ground states to reactive $^3C^*$ with species-specific energy levels (Canonica et al., 1995; Yu et al., 2014). $^3C^*$ is not a single photooxidant. Instead, $^3C^*$ is comprised of a variety of species with a range of reactivities (McNeill and Canonica, 2016). Some $^3C^*$ species can react rapidly with organic compounds (e.g., phenolic compounds and anilines) through single-electron transfer and proton-coupled electron transfer reactions (Lathioor and Leigh, 2006; Erickson et al., 2015). Some $^3C^*$ species can also react with organic compounds (e.g., aromatic amino acids) through hydrogen abstraction reactions (Walling and Gibian, 1965; Tsentalovich et al., 2002). In addition, energy transfer from $^3C^*$ to molecular oxygen ($^3O_2$) leads to the formation of $^1O_2^*$ (Herzberg and Herzberg, 1947). This reaction occurs rapidly under ambient conditions for most $^3C^*$ species since the energy required for $^3O_2 \rightarrow {}^1\Delta_g$ is only 94 kJ mol^{-1} (Zepp et al., 1985; Wilkinson et al., 1993; McNeill and Canonica, 2016). $^1O_2^*$ typically reacts with electron-rich/unsaturated species (e.g., alkenes, cyclic dienes, polycyclic aromatic hydrocarbons) through addition reactions (Ghogare and Greer, 2016; Kaur and Anastasio, 2017; Nolte and Peijnenburg, 2018; Manfrin et al., 2019; Barrios et al., 2021). The production of $^3C^*$ and $^1O_2^*$ are influenced by both the concentrations (i.e., quantity) and quantum yields (i.e., quality) of BrC chromophores (Bogler et al., 2022). The quantum yield, which describes the efficiency of oxidant photosensitization, can be obtained from dividing the number of moles of oxidant generated by the number of moles of photons absorbed by the photosensitizer. The relative importance of the quantity vs. quality of BrC chromophores in the production of $^3C^*$ and $^1O_2^*$ depends on the BrC source.

Aqueous reactions between organic compounds and photooxidants play key roles in forming and transforming secondary organic aerosols (SOA). Understanding the significance and contributions of these reactions to the SOA budget necessitates knowledge of the steady-state concentrations and quantum yields of the photooxidants. Out of all the photooxidants, $\cdot OH$ production in various atmospheric aqueous phases has been the most widely investigated (Arakaki and Faust, 1998; Arakaki et al., 1999, 2006, 2013; Anastasio and McGregor, 2001; Anastasio and Jordan, 2004; Anastasio and Newberg, 2007; Kaur and Anastasio, 2017; Kaur et al., 2019; Manfrin et al., 2019; Leresche et al., 2021; Ma et al., 2023b). $\cdot OH$ can be photochemically produced from BrC (Chen et al., 2021; Li et al., 2022) and other photolabile compounds such as inorganic nitrate, nitrite, and metal-organic complexes (Kaur and Anastasio, 2017; Kaur et al., 2019; Leresche et al., 2021; Ma et al., 2023b). There has been considerably fewer measurements of $^3C^*$ and $^1O_2^*$ production in atmospheric aqueous phases.

So far, several studies have measured $^1O_2^*$ production in cloud water (Faust and Allen, 1992), fog water (Anastasio and McGregor, 2001; Kaur and Anastasio, 2017), rain water (Albinet et al., 2010), and particulate matter (PM) extracts (Cote et al., 2018; Kaur et al., 2019; Manfrin et al., 2019; Leresche et al., 2021; Bogler et al., 2022; Ma et al., 2023b). $^1O_2^*$ originates

from a $^3C^*$ molecule, and therefore measuring both $^1O_2^*$ and its $^3C^*$ precursor is important. However, there has only been four investigations of $^3C^*$ production in atmospheric aqueous phases (Kaur and Anastasio, 2018; Kaur et al., 2019; Chen et al., 2021; Ma et al., 2023b). These studies showed that the concentrations of $^3C^*$ (10^{-16} to 10^{-13} M) and $^1O_2^*$ (10^{-14} to 10^{-12} M) produced are typically 2 to 4 orders of magnitude larger than the concentrations of $\cdot$OH (10^{-17} to 10^{-15} M) produced. Thus, despite the reactivity of $^3C^*$ and $^1O_2^*$ being substantially lower than $\cdot$OH, $^3C^*$ and $^1O_2^*$ can play important roles in aqueous SOA formation and transformation due to their large concentrations.

Spatiotemporal measurements of photooxidant production in atmospheric aqueous phases are important to understand how aqueous reactions between organic compounds and photooxidants can change as a function of season and of location. Leresche et al. (2021) measured $\cdot$OH and $^1O_2^*$ production in illuminated extracts of $PM_{2.5}$ collected during the winter, spring, and summer seasons in urban and rural settings in Colorado, USA, while Bogler et al. (2022) measured $^1O_2^*$ production in illuminated extracts of PM_{10} collected year-round at a rural site and a suburban site in Switzerland. The two studies highlighted the roles that seasonality and/or local anthropogenic activities play in influencing photooxidant production. At present, investigations of photooxidant production in atmospheric aqueous phases have been restricted to North America and Europe. Given the important role that aqueous photochemistry plays in forming and transforming SOA in many regions, there is, therefore, a need to investigate the spatiotemporal variations of photooxidant production in atmospheric aqueous phases in regions outside of North America and Europe.

In this work, we investigated the production of $^3C^*$ and $^1O_2^*$ in illuminated extracts of $PM_{2.5}$ collected during different seasons at three sites (two urban and one semi-rural) in Hong Kong. Hong Kong is a densely populated coastal city located on the east of the Pearl River Delta (PRD) in South China. Its seasonal meteorological conditions and air quality are strongly influenced by the East Asian monsoon (Yihui and Chan, 2005). Clean, marine air masses are transported from southwestern sea areas to Hong Kong in the summer, whereas polluted air mass are transported from northern continental areas to Hong Kong in mid-fall and winter (Tanner and Law, 2002). Local sources are the main contributors to summer $PM_{2.5}$, whereas regional sources are the main contributors to winter $PM_{2.5}$ (Pathak et al., 2003; Louie et al., 2005; Louie, 2005; Huang et al., 2014; Li et al., 2015; Wong et al., 2020). The main objectives of this study are to (1) characterize the steady-state concentrations and quantum yields of $^3C^*$ and $^1O_2^*$, and (2) determine how location and seasonality influence $^3C^*$ and $^1O_2^*$ production in Hong Kong. This work presents the first spatiotemporal measurements of photooxidants produced in atmospheric aerosols in East Asia. Results from this study provide insights into the levels of $^3C^*$ and $^1O_2^*$ produced in $PM_{2.5}$ in the South China region, which will be useful for improving our understanding of aqueous organic aerosol photochemical processes in this region.

2 Methods

2.1 PM$_{2.5}$ filter sampling and extraction

2.1.1 Sampling locations

The year-round sampling campaign took place from December 2020 to December 2021 in Hong Kong. The three sites were the City University of Hong Kong campus (CU, 22°20'05"N, 114°10'23"E), and the air quality monitoring stations at Tsuen Wan (TW, 22°20'17"N, 114°06'52"E) and Hok Tsui (HT, 22°12'33"N, 114°15'12"E) (Figure 1). The CU and TW sites are located in urban areas with many residential and commercial (and industrial for TW) activities. Since the semi-rural coastal HT site is located away from local emission sources (approximately 6 km away from the closest urban area), it was mostly used as a receptor site to monitor air pollution originating from sources outside of Hong Kong in past studies (Tanner and Law, 2002; Li et al., 2018). In Hong Kong, winter nominally runs from December to February, spring runs from March to May, summer runs from June to August, and fall runs from September to November. Sampling activities at each site took place for approximately one month during each season (Table S1).
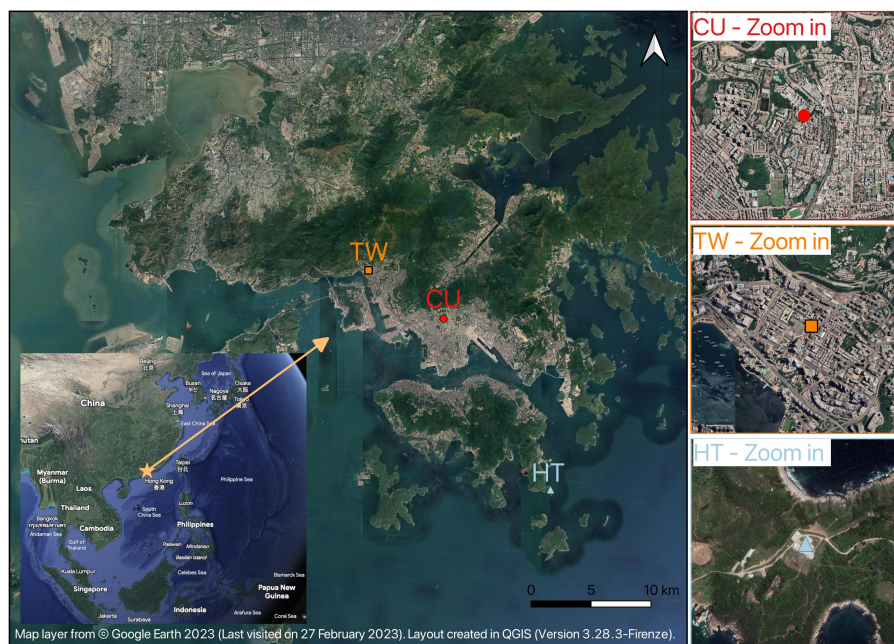
Figure 1. Satellite image of the three sites in Hong Kong. CU, TW, HT are short for the City University of Hong Kong campus, Tsuen Wan, and Hok Tsui sites, respectively.

2.1.2 Sampling and extraction protocols

PM$_{2.5}$ was collected on three prebaked (550 °C for 12 h) 47 mm diameter quartz filters (Pall Tissuquartz^{TM}, 2500 QAT-UP) using a custom-built medium-volume sampler with a PM$_{2.5}$ inlet. Ambient air was sampled onto each quartz filter at 30 L min^{-1}. The sampler was deployed at ground level at the CU and HT sites, and on a 17 m rooftop at the TW site. PM$_{2.5}$ samples were collected continuously for 72 hours every third day. The filter samples were stored in resealable bags at -25 °C until the day of extraction. Blank filter samples were generated the same way as the ambient filter samples, except the sampler pump for this channel was switched off during sampling.

Each filter was extracted in 7 mL Milli-Q water inside a 15 mL sterile centrifuge tube (JET BIOFIL$^{®}$) by vortexing for 4 minutes (MX-S DLAB, medium high power). The disintegrated filter parts were removed from the extracts by filtration using 0.22 µm pore size nylon syringe filters (Nylon66, Jinteng$^{®}$). The filtered extracts were stored in amber vials at 4 °C in a refrigerator until the day of photochemical experiments. The maximum amount of time for which the extracts were stored in the refrigerator (i.e., from the day of extraction to the day of project completion) is 6 months. We compared the WSOC and light absorption measurements performed on the extracts within a week of extraction vs. after the photochemical experiments have concluded, and observed minimal changes in the WSOC and light absorption properties of the extracts.

Extracts from three consecutive sampling periods (9 filters in 9 days) were aggregated to minimize daily variability. This procedure resulted in roughly 3 aggregated extracts per season for each site, referred to by the site and sampling start date. For example, sample CU041220 refers to extracts of filters collected from 4 Dec 2020 to 13 Dec 2020 at the CU site. Due to sampler pump malfunction, filters were not collected at the CU site from 18 June 2020 to 24 June 2020 and at the HT site from 18 April 2020 to 27 April 2020. In addition, some aggregated extracts were comprised only of two consecutive sampling periods (6 filters in 6 days) due to limited filter samples. It should be noted that all the aggregated extracts were further diluted with Milli-Q water by a factor of 2.22 for light absorption measurements and photochemical experiments. This was equivalent to extracting each filter with 15.54 mL Milli-Q water. The PM$_{2.5}$ mass to water mass ratios (PM$_{2.5}$ mass/H$_2$O mass) were calculated for each aggregated extract using the ambient PM$_{2.5}$ mass concentrations measured at or near the sampling sites by the Hong Kong Environmental Protection Department. Detailed information about the sampling periods, allocation of aggregated extracts, and calculation of PM$_{2.5}$ mass/H$_2$O mass values are shown in Table S1.

2.2 Light absorption measurements

The UV-Visible absorbance spectra of the extracts were obtained in 1-nm increments using a UV-VIS-NIR spectrophotometer (Shimadzu UV-3600) with Milli-Q water as the reference sample. The spectra were corrected by subtracting spectra from the field blanks and the average absorbance between 700 to 800 nm (Ossola et al., 2021). The decadic absorption coefficient (α_λ, cm^{-1}) was calculated using the following equation:

$$\alpha_\lambda = \frac{A_\lambda}{l} \tag{1}$$

where A_λ is the dimensionless absorbance of extracts at wavelength λ, and l is the optical path length (1 cm) of the cuvette.

130 The rate of light absorption (R_{abs}, mol-photons L^{-1} s^{-1}) of each extract was calculated using the following equation:

$$R_{abs} = \frac{10^3}{d} \sum_{290\,nm}^{600\,nm} I_{0,\lambda}(1 - 10^{-\alpha_\lambda d})\Delta\lambda \tag{2}$$

where d is the path length of the light through the quartz tubes used in the photochemical experiments (cm), 10^3 is for units conversion (cm^3 L^{-1}), $I_{0,\lambda}$ (mol-photons nm^{-1} s^{-1} cm^{-2}) is the absolute irradiance of the light source at wavelength λ, and $\Delta\lambda$ is the interval of wavelength (1 nm). d was assumed to be equals to the inner diameter of the quartz tubes (1.25 cm). We

135 acknowledge that the actual optical path length may be slightly different from the inner diameter of the quartz tubes used in our calculations. Nevertheless, we do not expect these differences to affect our R_{abs} and quantum yield calculations significantly (Ossola et al., 2021). For instance, using $d = 1$ cm will cause the calculated quantum yields to decrease, on average, only by 0.53 % relative to quantum yields calculated using $d = 1.25$ cm. A wavelength range of 290 to 600 nm was used to cover both the output of the photoreactor lamps and light absorption range of all the extracts (Figure S1). R_{abs} was not corrected for light

140 screening (i.e., inner filter effect) since the absorbance coefficients of all the extracts were below 0.1 cm^{-1} in the UVA range. The wavelength-dependent mass absorption coefficients for the WSOC (MAC$_\lambda$, m^2 g-C^{-1}) in the extracts were calculated using the following equation:

$$\text{MAC}_\lambda = \frac{\alpha_\lambda \times \ln(10)}{[\text{WSOC}] \times 10^{-2}} \tag{3}$$

where $\ln(10)$ is the base conversion factor, 10^{-2} is for unit conversion, and [WSOC] (in mg-C L^{-1}) is the concentration of the

145 WSOC in each extract (Table S2) measured by a TOC Analyzer (Shimadzu TOC-V CSH). It should be noted that the mass ratio of the organic material (OM) to organic carbon (OC) in PM$_{2.5}$ in Hong Kong is approximately 2.1 (Chen and Yu, 2007). Thus, the calculated MAC$_\lambda$ values would be halved had they been normalized by [OM] instead of [WSOC]. Section S1 describes the detection methods of inorganic ions in the extracts.

Various light absorption properties were obtained for each extract based on their absorbance and WSOC measurements

150 (Table S3). The α_{300} is the UV absorption coefficients at 300 nm. SUVA$_{254}$ and SUVA$_{365}$ are the specific UV absorbance obtained from dividing the UV absorption coefficients at 254 nm and at 365 nm (α_{254} and α_{365}, respectively) by [WSOC]. The AAE is the absorption Ångström exponent, which can be calculated using the following equation:

$$\text{AAE} = -\frac{\ln(\alpha_{\lambda_2}/\alpha_{\lambda_1})}{\ln(\lambda_2/\lambda_1)} \tag{4}$$

The AAE values were obtained from the negative of the slope of the linear plot of $\ln(\alpha_\lambda)$ vs. $\ln(\lambda)$ in the range of 300 to 450 nm

155 (26 extracts) or 300 to 350 nm (8 extracts). The narrower wavelength range was used for extracts that had very low absorbance at the long wavelengths to ensure good linearity.

2.3 Chemicals used in photochemical experiments

The chemical probe for $^1O_2^*$, furfuryl alcohol (98 %), was purchased from Acros Organics and was distilled under vacuum before being prepared into a 100 µM stock solution. Deuterium oxide (D$_2$O, 99 % atom D) was purchased from Sigma Aldrich.

160 The chemical probe for $^3C^*$, 2,6-dimethoxyphenol (syringol, 98 %), was purchased from J&K Scientific. The chemical acti-
nometer, 2-nitrobenzaldhyde (2-NB, 98 %), was purchased from J&K Scientific. Preparation of all chemical solutions and
dilution of the extracts were performed using ultrapure Milli-Q water (Merck, resistivity of 18.2 MΩ cm).

2.4 Photochemical experiments

Irradiation experiments were conducted in a Rayonet photoreactor (RPR-200, Southern New England Ultraviolet Co.) equipped
165 with 12 UVA lamps (RPR-3500Å, Southern New England Ultraviolet Co.). The spectral irradiance is shown in Figure S2. The
procedure used to determine the photon flux is described in Section S2. In a typical photochemical experiment, quartz tubes
containing 5 mL of extract spiked with a probe compound (10 μM) were placed on a merry-go-round sample holder (RMA-500,
Southern New England Ultraviolet Co.) in the middle of the photoreactor for continuous illumination. The chemical probes
for $^1O_2^*$ and $^3C^*$ were furfuryl alcohol (Appiani et al., 2017) and syringol (Kaur and Anastasio, 2018; Kaur et al., 2019; Ma
170 et al., 2023b), respectively. The temperature inside the photoreactor during the experiment was maintained at 26 ± 1 °C by
a cooling fan positioned at the bottom of the photoreactor. Aliquots of the solutions were removed at different reaction times
to monitor the loss of the chemical probe using a ultrahigh-pressure liquid chromatography system coupled to a photodiode
array detector (UPLC-PDA, Waters ACQUITY H-Class). Separation of the chemical probes, furfuryl alcohol and syringol, was
achieved using a Phenomenex Kinetex polar C18 column (2.6 μm, 100 × 2.1 mm) and elution at 0.3 mL min^{-1} with Milli-Q
175 water/acetonitrile ratios of 9:1 and 8:2, respectively. The PDA detection wavelengths for furfuryl alcohol and syringol were 216
nm and 210 nm, respectively. Control experiments showed that syringol and furfuryl alcohol loss in illuminated Milli-Q water
and field blank extracts were mostly minimal and the differences were within experimental errors (Figure S3). This indicated
that $^3C^*$ and $^1O_2^*$ production were negligible in the background samples.

2.5 Quantification of steady-state concentrations, formation rates, and quantum yields of $^1O_2^*$

180 Furfuryl alcohol was used as the $^1O_2^*$ chemical probe (Appiani et al., 2017). The kinetic solvent isotope effect (KSIE) was used
to account for furfuryl alcohol degradation by oxidants other than $^1O_2^*$ in the quantification of the steady-state concentrations
of $^1O_2^*$ ($[^1O_2^*]_{ss}$) in the extracts (Davis et al., 2018). These experiments involved comparing the decays of furfuryl alcohol in
pure water (H_2O) vs. in heavy water (D_2O) (Haag and Hoigne, 1986; Allen et al., 1996; Anastasio and McGregor, 2001; Kaur
and Anastasio, 2017; Kaur et al., 2019; Ma et al., 2023b). The extracts were prepared in Milli-Q water or in a mixture of 1:1
185 Milli-Q water/D_2O (v/v), wherein they were spiked with 10 μM furfuryl alcohol. The furfuryl alcohol decay followed pseudo
first-order kinetics (Figure S4). Their rate constants were used to calculate $[^1O_2^*]_{ss}$ as follows:

$$[^1O_2^*]_{ss} = \frac{k'_{FFA,D_2O} - k'_{FFA,H_2O}}{k_{rxn}^{FFA+^1O_2^*} \times \frac{k_{d,H_2O} - k_{d,D_2O}}{k_{d,H_2O} + k_{d,D_2O}}} \tag{5}$$

where k'_{FFA,D_2O} and k'_{FFA,H_2O} are the pseudo first-order rate constants of furfuryl alcohol loss in the 1:1 Milli-Q water/D_2O (v/v)
mixture and in Milli-Q water, respectively, determined from the slopes of the linear plot of $\ln([FFA]_t/[FFA]_0)$ vs. irradiation
190 time (Figure S4), $k_{rxn}^{FFA+^1O_2^*}$ is the second order rate constant of FFA with $^1O_2^*$ at 26 °C (1.084×10^8 M^{-1} s^{-1}) (Appiani et al.,

2017), and k_{d,H_2O} and k_{d,D_2O} are the $^1O_2^*$ deactivation rates in pure H_2O (2.81×10^5 s^{-1}) and pure D_2O (1.57×10^4 s^{-1}), respectively (Davis et al., 2018). Since the furfuryl alcohol decay from direct photolysis was minimal, the photolysis rate ($7.58 \pm 0.83 \times 10^{-7}$ s^{-1}, Figure S3) was not used to correct the k'_{obs,D_2O} and k'_{obs,H_2O} values.

The formation rate of $^1O_2^*$ ($R_{f,^1O_2^*}$) was calculated as follows:

195 $$R_{f,^1O_2^*} = [^1O_2^*]_{ss} \times k_{d,H_2O} \tag{6}$$

The quantum yield of $^1O_2^*$ ($\Phi_{^1O_2^*}$) was calculated as follows:

$$\Phi_{^1O_2^*} = \frac{R_{f,^1O_2^*}}{R_{abs}} \tag{7}$$

2.6 Quantification of steady-state concentrations, formation rates, and quantum yields of $^3C^*$

We used syringol as the sole $^3C^*$ chemical probe. However, we acknowledge that due to the chemical complexity of $^3C^*$

200 species, a single chemical probe has limitations to quantify all the $^3C^*$ species (McNeill and Canonica, 2016; Maizel and Remucal, 2017). While some studies have used multiple probes (and thus, performed multiple photochemical experiments) to better constrain $^3C^*$ measurements (Kaur and Anastasio, 2018; Kaur et al., 2019; Ma et al., 2023b), we were unable to do so in our study due to insufficient extract volumes for additional photochemical experiments. Thus, only a subset of $^3C^*$ species that oxidize syringol were quantified in this study (Kaur and Anastasio, 2018).

205 The syringol decays followed pseudo first-order kinetics (Figure S5). The syringol decay rates were used to calculate the steady-state concentrations of $^3C^*$ ($[^3C^*]_{ss}$) as follows:

$$[^3C^*]_{ss} = \frac{1}{4} \sum_{i=1}^{i=4} \frac{k'_{SYR} - k_{rxn}^{SYR+^1O_2^*} \times [^1O_2^*]_{ss} - j_{SYR}}{k_{rxn}^{SYR+model\,^3C_i^*}} \tag{8}$$

where k'_{SYR} is the pseudo first-order rate constant of syringol loss determined from the slope of the linear plot of $\ln([SYR]_t/[SYR]_0)$ vs. irradiation time (Figure S5), $k_{rxn}^{SYR+^1O_2^*}$ is the second order rate constant between syringol and $^1O_2^*$ (($3.6 \pm 0.7) \times 10^7$ M^{-1}

210 s^{-1}) (Tratnyek and Hoigne, 1991), j_{SYR} is the first order loss rate of syringol in field blank samples ($2.62 \pm 0.12 \times 10^{-6}$ s^{-1}, Figure S3), and $k_{rxn}^{SYR+model\,^3C_i^*}$ is the second order rate constant between syringol and a model $^3C^*$ species (Table S4). Since $^3C^*$ comprises of a variety of species with a range of reactivities, there is no single value for the rate constant of syringol with $^3C^*$. Thus, the $[^3C^*]_{ss}$ value for each extract was calculated by taking the average of the $[^3C^*]_{ss}$ values calculated using four model $^3C^*$ species (2-acetonaphthone ($^32AN^*$), 3'-methoxyacetophenone ($^33MAP^*$), 3,4-dimethoxybenzaldehyde ($^3DMB^*$),

215 and benzophenone ($^3BP^*$)) which were chosen to cover the range of $^3C^*$ reactivities in atmospheric samples. While previous studies performed ·OH photochemical experiments to correct for the reaction between syringol and ·OH in their $[^3C^*]_{ss}$ calculations (Kaur and Anastasio, 2018; Kaur et al., 2019; Ma et al., 2023c), we did not do so in our study due to insufficient extract volumes for additional photochemical experiments. However, previous studies have reported that the contribution of both ·OH and $^1O_2^*$ to the loss of syringol were < 20 % for the measurement of $[^3C^*]_{ss}$ in fog water (Kaur and Anastasio, 2018) and PM

220 extracts (Kaur et al., 2019).

The formation rate of $^3C^*$ ($R_{f,^3C^*}$) was calculated as follows:

$$R_{f,^3C^*} = [^3C^*]_{ss} \times (k_{q,O_2}[O_2(aq)] + k_{rxn+q}^{^3C^*+WSOC}[WSOC]) \tag{9}$$

where k_{q,O_2} is the average second order rate constant for the four model $^3C^*$ species quenching via energy transfer to dissolved O_2 (2.8×10^9 M^{-1} s^{-1}) (Canonica et al., 2000; Kaur and Anastasio, 2018), [O_2 (aq)] is the dissolved O_2 concentration in

225 water at 26 °C (2.53×10^{-4} M) (Rounds et al., 2006), $k_{rxn+q}^{^3C^*+WSOC}$ is the estimated overall rate constant for $^3C^*$ loss (i.e., reaction and quenching) due to WSOC (9.3×10^7 L mol-C^{-1} s^{-1}) (Kaur et al., 2019), and [WSOC] (in mg-C L^{-1}) is the concentration of WSOC in each extract (Table S2).

The quantum yield of $^3C^*$ ($\Phi_{^3C^*}$) was calculated as follows:

$$\Phi_{^3C^*} = \frac{R_{f,^3C^*}}{R_{abs}} \tag{10}$$

230 Uncertainties were propagated from the measured decay kinetics of furfuryl alcohol and syringol in triplicate photochemical experiments and one standard deviation of the literature second order rate constants. Statistics and linear regression analyses were performed using Prism 8.

3 Results and discussion

3.1 Characteristics of the extracts

235 #### 3.1.1 WSOC and light absorption properties

The same sampling flow rate (30 L min^{-1}) and period (72 h) were used to collect all the filters and the same dilution ratio (i.e., equivalent to extracting each filter in 15.54 mL Milli-Q water) was used to prepare all the extracts. This allowed us to compare the WSOC concentrations and light absorption properties across the extracts. The PM$_{2.5}$ mass/H$_2$O mass ratios for the extracts (Table S1) ranged from 1.86×10^{-5} to 2.14×10^{-4} µg PM$_{2.5}$/µg H$_2$O, which were close to fog and cloud water conditions

240 but were much more diluted compared to aerosol liquid water conditions (ca. 1 µg PM/ µg H$_2$O) (Liao and Seinfeld, 2005; Herrmann et al., 2015; Nguyen et al., 2016; Seinfeld and Pandis, 2016). The concentrations of WSOC in the extracts ranged from 3.8 to 25.7 mg-C L^{-1}, with a study average of 13.7 mg-C L^{-1} (Table S2), which were close to the WSOC concentrations previously measured in fog and ground base clouds (Herckes et al., 2013). The concentrations of WSOC in the extracts were linearly correlated (SLR $r^2 = 0.93$) with the PM$_{2.5}$ mass/H$_2$O mass ratios (Figure 2).

245 Converted to the carbon mass concentration in air, the study average WSOC concentration (1.7 ± 0.8 µg m^{-3}) was close to previously reported values at another Hong Kong urban site (1.8 ± 1.1 µg m^{-3}) and the semi-rural site HT (1.3 ± 1.1 µg m^{-3}) in PM$_{2.5}$ (Huang et al., 2014). The WSOC concentration had a noticeable seasonal trend, wherein the concentrations were higher in the fall and winter extracts and the lowest concentrations were measured in the summer extracts (Table S2). The seasonal variations in the WSOC concentration in PM$_{2.5}$ could be attributed to the seasonal variations in long-range air

250 mass transport influenced by the East Asian monsoon system (Huang et al., 2014; Zhang et al., 2018; Chow et al., 2022).
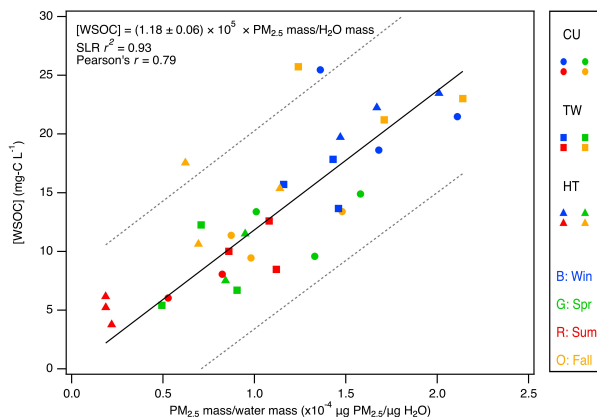
Figure 2. The WSOC concentration as a function of the $PM_{2.5}$ mass/water mass ratio for the extracts. Blue, green, red, and orange symbols denote the winter, spring, summer, and fall samples, respectively. The dashed lines represent 95 % prediction bands. The SLR r^2 and Pearson's r are the coefficient of determination for simple linear regression and the Pearson correlation coefficient, respectively.

Air masses originating mainly from polluted continental areas located north of Hong Kong contributed to the high $PM_{2.5}$ and WSOC concentrations in fall and winter (Figures S6 to S8). In the summer, air masses originate from clean marine regions located south of Hong Kong instead. These summer marine air masses generally have low $PM_{2.5}$ and WSOC concentrations. This results in Hong Kong having substantially lower $PM_{2.5}$ and WSOC concentrations in the summer compared to the fall and winter. Consequently, regional sources are the main $PM_{2.5}$ contributors in fall and winter, whereas local sources are the main $PM_{2.5}$ contributors in the summer (Huang et al., 2014; Zhang et al., 2018; Chow et al., 2022).

All the extracts had absorbance from the near-UV to the visible region, indicating the presence of BrC and the potential of generating $^1O_2^*$ and $^3C^*$ in all extracts. The absorption coefficient, α_λ, and mass absorption coefficient, MAC_λ, declined exponentially with λ for all the extracts (Figure 3). The average values of the absorption coefficient and mass absorption coefficient at 300 nm (α_{300} and MAC_{300}) indicated that, on average, the absorbance for the urban CU and TW extracts were slightly higher than the absorbance for the semi-rural HT extracts (Table 1). Upon grouping the α_{300} and MAC_{300} datasets based on seasonality irrespective of the sampling location, we observed noticeable differences in the seasonal α_{300} and MAC_{300} values (Table 2). The average seasonal α_{300} and MAC_{300} values followed similar trends: winter > fall > spring > summer. Since the MAC_{300} accounts for WSOC dilution (Equation 3), the higher MAC_{300} values in the winter extracts indicated that the water-soluble organic compounds in winter $PM_{2.5}$ were more strongly absorbing and/or were less diluted with weakly absorbing water-soluble organic compounds compared to the $PM_{2.5}$ from the other three seasons.

The AAE describes the spectral dependence of light absorption, and is typically used to indicate BrC contribution to the total absorption of aerosols (Helin et al., 2021). The AAE value for black carbon is typically close to 1, while AAE values larger than 1 indicate the presence of BrC (Kirchstetter et al., 2004). All the AAE values were larger than 1, thus indicating the omnipresence of BrC. The AAE values were fairly similar among the three sites (Table 1) and across the four seasons
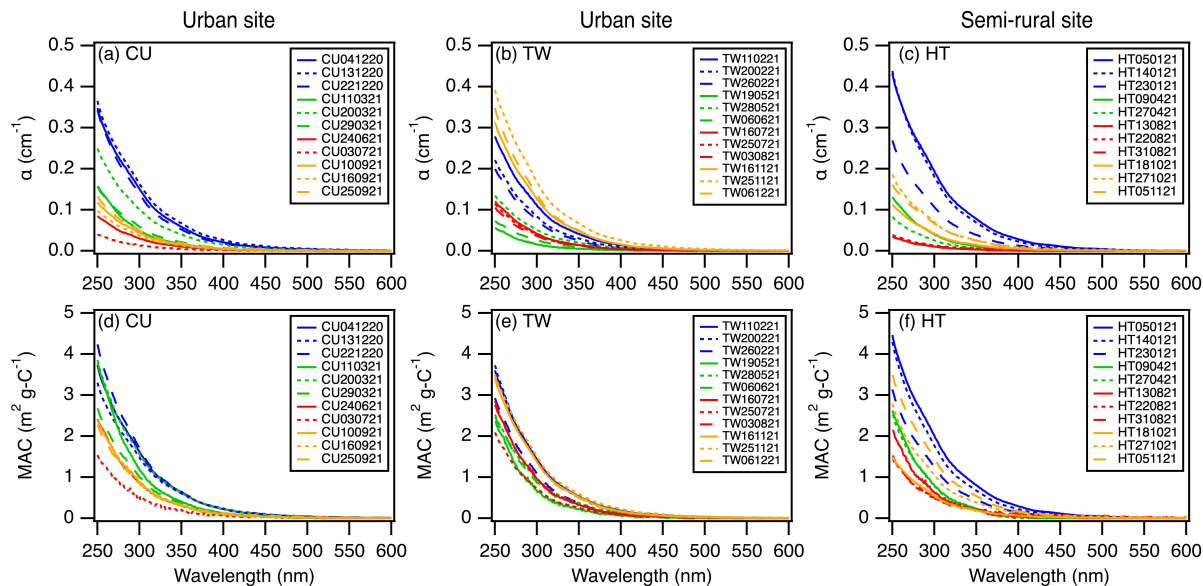
Figure 3. (a to c) α_λ and (d to f) MAC_λ of $PM_{2.5}$ extracts from CU, TW, and HT, respectively. The lines in blue, green, red, and orange indicated samples collected during the winter, spring, summer, and fall seasons, respectively.

(Table 2). The R_{abs} values summarize the light absorption rates ranging from 290 to 600 nm. R_{abs} was linearly correlated with the WSOC concentration, with Pearson's *r* values between 0.88 and 0.97 for the three sites (Figure S9). The good correlation between R_{abs} and the WSOC concentration implied that water-soluble BrC was likely the main contributor to the total light absorption.

275    $SUVA_{254}$ and $SUVA_{365}$, which are the specific UV absorbance obtained from dividing the absorption coefficients at 254 nm and at 365 nm by the WSOC concentration, are commonly used as proxies for organic matter aromaticity. Higher $SUVA_{254}$ and $SUVA_{365}$ values indicate enhanced aromaticity (Weishaar et al., 2003). As expected, the $SUVA_{254}$ values for the three sites were higher than the $SUVA_{365}$ values. These average $SUVA_{254}$ and $SUVA_{365}$ values for the three sites indicated that the organic matter in the urban CU and TW extracts, on average, had higher aromaticity than those in the semi-rural HT extracts

280   (Table 1). It is possible that the observed higher absorbance and aromaticity in the urban CU and TW extracts were due to the presence of oxygenated aromatic compounds (e.g., highly substituted phenolic compounds) from local anthropogenic sources such as vehicle emissions, combustion-related (e.g., cooking, power generation and usage) activities, and solvent usage (Guo et al., 2003; Chen et al., 2017; Cui et al., 2018; Bilal et al., 2019). Upon grouping the $SUVA_{254}$ and $SUVA_{365}$ datasets based on seasonality irrespective of the sampling location, the average seasonal $SUVA_{254}$ and $SUVA_{365}$ values indicated that the organic

285   matter in the fall and winter extracts, on average, had higher aromaticity than those in the spring and summer extracts (Table 2). The higher aromaticity in the fall and winter extracts was likely due to strong biomass burning contributions to ambient fall and winter $PM_{2.5}$. Hong Kong generally has low levels of biomass burning activities. However, fall and winter $PM_{2.5}$ in continental areas north of Hong Kong (e.g., parts of Mainland China) can have substantial contributions from biomass burning, especially

in rural areas where residential biomass burning are used for intensive heating purposes (Chen et al., 2017). It is possible that biomass burning-influenced air masses from these northern continental areas were transported to Hong Kong during fall and winter, and consequently contributed to the higher aromaticity in these extracts.

3.1.2   Site and seasonal variations in WSOC and light absorption properties

We hypothesized that the site and seasonal variations in the WSOC concentration and light absorption properties of water-soluble BrC in the $PM_{2.5}$ drove the site and seasonal variations in $^3C^*$ and $^1O_2^*$ production. Thus, we examined the site and seasonal variations in the WSOC and light absorption properties of the extracts. The above comparisons of the average WSOC concentration, α_{300}, MAC_{300}, $SUVA_{254}$, and $SUVA_{365}$ values of the urban CU and TW extracts vs. semi-rural HT extracts indicated that, on average, $PM_{2.5}$ at CU and TW had slightly higher concentrations of and/or more absorbing water-soluble BrC comprised of organic matter of high aromaticity compared to $PM_{2.5}$ at HT. However, statistics performed on the WSOC concentration, α_{300}, MAC_{300}, AAE, R_{abs}, $SUVA_{254}$, and $SUVA_{365}$ datasets showed that their variations between the three sites were not significant ($p > 0.05$) (Table S3). These results indicated that the locations (i.e., urban vs. semi-rural) did not have a significant influence on the concentration of WSOC and light absorption properties of water-soluble BrC in $PM_{2.5}$.

Since the locations did not have a significant influence on the the WSOC concentration and light absorption properties of water-soluble BrC, we combined the datasets from the three sites and separated them based on seasonality. Despite the spread in their seasonal values, seasonal variations in the WSOC concentration, α_{300}, MAC_{300}, R_{abs}, $SUVA_{254}$, and $SUVA_{365}$ values were statistically significant ($p < 0.05$) (Figure S10). This implied that the seasonal variations in long-range air mass transport had a significant influence on the WSOC concentration and light absorption properties of water-soluble BrC. The WSOC concentration, α_{300}, MAC_{300}, R_{abs}, $SUVA_{254}$, and $SUVA_{365}$ had noticeably similar trends: winter > fall > spring > summer. These seasonal trends indicated that winter and fall $PM_{2.5}$ had higher concentrations of and/or more absorbing water-soluble BrC comprised of organic matter of high aromaticity compared to the summer and spring $PM_{2.5}$. Based on the seasonal variations in long-range air mass transport during the study (Figures S6 to S8), regional sources were important contributors to water-soluble BrC comprised of organic matter of high aromaticity in winter and fall $PM_{2.5}$. Interestingly, seasonal variations in the AAE values were not statistically significant ($p > 0.05$). While it is unclear why seasonal trends were not observed for the AAE values in our study, other studies have similarly reported the lack of seasonal trends in the AAE values (Du et al., 2014; Ma et al., 2023b).

3.2 $^1O_2^*$ and $^3C^*$ production during extract illumination

3.2.1 $^1O_2^*$

The pseudo first-order decay rate constants of furfuryl alcohol ($^1O_2^*$ chemical probe) in photochemical experiments (Figure S4) were used to determine the steady-state concentrations of $^1O_2^*$, $[^1O_2^*]_{ss}$ (Equation 5). The $[^1O_2^*]_{ss}$ values spanned two orders of magnitude, ranging from 1.56×10^{-14} to 1.35×10^{-12} M, with a study average of $(4.02 \pm 3.52) \times 10^{-13}$ M (Table S5). These $[^1O_2^*]_{ss}$ values were in line with those previously measured in atmospheric samples (10^{-15} to 10^{-12} M) (Table S7).

Table 1. Summary of WSOC concentration, light absorption properties, steady-sate concentrations, and quantum yields of $^1O_2^*$ and $^3C^*$ for the CU, TW, and HT sites.

Parameters	Units	CU		TW		HT	
		Range	Average	Range	Average	Range	Average
[WSOC]	mg-C L^{-1}	6.03-25.46	13.79 ± 5.96	5.41-25.73	14.38 ± 6.51	3.76-23.46	13.01 ± 7.05
α_{300}	cm^{-1}	0.01-0.16	0.08 ± 0.05	0.02-0.17	0.08 ± 0.05	0.01-0.19	0.07 ± 0.07
R_{abs}	×10^{-6} mol-photons L^{-1} s^{-1}	0.37-5.23	2.23 ± 1.66	0.39-5.17	2.11 ± 1.47	0.20-5.82	1.91 ± 1.93
MAC$_{300}$	m^2 g-C^{-1}	0.52-1.49	1.15 ± 0.39	0.68-1.51	1.12 ± 0.29	0.64-2.01	1.03 ± 0.53
SUVA$_{254}$	L mg-C^{-1} m^{-1}	0.61-1.33	1.19 ± 0.35	0.95-1.43	1.20 ± 0.22	0.85-1.80	1.09 ± 0.43
SUVA$_{365}$	L mg-C^{-1} m^{-1}	0.05-0.20	0.13 ± 0.05	0.07-0.19	0.13 ± 0.04	0.05-0.26	0.11 ± 0.07
AAE		6.45-8.30	7.38 ± 0.56	6.82-8.07	7.40 ± 0.45	5.31-8.56	7.19 ± 1.01
[$^1O_2^*$]$_{ss}$	×10^{-13} M	0.16-8.22	3.41 ± 2.54	0.33-8.88	4.30 ± 2.97	0.23-13.47	4.32 ± 4.93
$R_{f,^1O_2^*}$/[WSOC]	× 10^{-9} M s^{-1} L mg-C^{-1}	0.73-10.75	6.14±2.75	1.73-10.84	7.58±3.34	1.04-18.44	7.07±6.29
$\Phi_{^1O_2^*}$	%	1.19-7.21	4.31 ± 1.70	2.11-9.54	5.60 ± 2.31	1.35-13.74	5.62 ± 3.58
[$^3C^*$]$_{ss}$	×10^{-15} M	1.41-17.19	9.59 ± 5.16	0.35-27.27	7.76 ± 7.19	0.29-80.77	15.73±22.62
$R_{f,^3C^*}$/[WSOC]	× 10^{-10} M s^{-1} L mg-C^{-1}	1.77-8.99	5.76±2.80	0.48-24.93	5.31±6.64	0.42-43.53	8.57±11.93
$\Phi_{^3C^*}$	%	0.18-0.85	0.44 ± 0.26	0.06-2.28	0.47 ± 0.64	0.05-3.24	0.77 ± 0.91

Note: uncertainties are one standard deviation.

The [$^1O_2^*$]$_{ss}$ values were linearly correlated with two indicators of water-soluble BrC, WSOC concentration and α_{300}, with Pearson's r values of 0.88 and 0.92, respectively (Figures S11a and S11b). These correlations provided strong evidence that the production of $^1O_2^*$ was linked to water-soluble BrC. The large range in the [$^1O_2^*$]$_{ss}$ values was likely due to the variations in the absorbance in the BrC chromophores (Figure 3).

The formation rates of $^1O_2^*$, $R_{f,^1O_2^*}$, ranged from 4.39×10^{-9} to 3.79×10^{-7} M s^{-1} (Table S5). Across all extracts, the $R_{f,^1O_2^*}$ was linearly correlated with R_{abs} (Figure S12a), which was consistent with water-soluble BrC being a source of $^1O_2^*$. The study average WSOC-normalized $R_{f,^1O_2^*}$ (($6.95 \pm 4.28) \times 10^{-9}$ M s^{-1} L mg-C^{-1}) was within a factor of 2 of previously reported values for PM$_{2.5}$ samples collected in urban and rural areas in Colorado, USA (Leresche et al., 2021) and for PM samples collected in biomass burning-influenced areas in California, USA (Kaur et al., 2019; Ma et al., 2023a). The quantum yields of $^1O_2^*$, $\Phi_{^1O_2^*}$, ranged from 0.77 to 13.74 %, with a study average of (5.12 ± 2.66) %, which was noticeably higher than previously reported $\Phi_{^1O_2^*}$ values for atmospheric PM samples (0.3 to 4.5 %) (Kaur and Anastasio, 2017; Manfrin et al., 2019; Kaur et al., 2019; Leresche et al., 2021; Bogler et al., 2022). This suggested that the water-soluble BrC in our extracts have higher $^1O_2^*$ photosensitization efficiencies compared to that in previous studies, which could be due to the different composition and age of water-soluble BrC in atmospheric PM in different locations. For instance, ozone is a major ground-level air pollutant in Hong Kong (Liao et al., 2021). Exposure to ambient ozone pollution could have led to higher $\Phi_{^1O_2^*}$ values due to the formation of quinone-like moieties from ozone aging of phenolic moieties present in water-soluble BrC (Leresche et al., 2019). It is also possible that the higher $\Phi_{^1O_2^*}$ values observed in our study could be due to differences in experimental conditions. For instance,

Table 2. Summary of WSOC concentration, light absorption properties, steady-state concentrations, and quantum yields of $^1O_2^*$ and $^3C^*$ for the four seasons.

Parameters	Winter		Spring		Summer		Fall	
	Range	Average	Range	Average	Range	Average	Range	Average
[WSOC]	13.66-25.46	19.80 ± 3.77	5.41-14.90	10.15 ± 3.40	3.76-12.59	7.54 ± 2.84	9.45-25.73	16.41 ± 5.83
α_{300}	0.08-0.19	0.13 ± 0.04	0.02-0.10	0.05 ± 0.03	0.01-0.04	0.03 ± 0.01	0.04-0.17	0.08 ± 0.05
R_{abs}	1.72-5.82	3.83 ± 1.40	0.33-3.14	1.23 ± 0.92	0.20-1.08	0.68 ± 0.34	1.01-5.17	2.35 ± 1.45
MAC_{300}	1.10-2.01	1.53 ± 0.28	0.68-1.56	0.99 ± 0.28	0.49-1.00	0.72 ± 0.21	0.55-1.51	1.11 ± 0.33
$SUVA_{254}$	1.18-1.80	1.49 ± 0.22	0.95-1.55	1.15 ± 0.24	0.58-1.14	0.84 ± 0.23	0.60-1.43	1.13 ± 0.29
$SUVA_{365}$	0.11-0.26	0.18 ± 0.04	0.05-0.20	0.10 ± 0.05	0.05-0.10	0.08 ± 0.02	0.06-0.19	0.13 ± 0.04
AAE	6.66-7.80	7.32 ± 0.36	6.86-8.56	7.51 ± 0.65	5.31-8.07	6.98 ± 1.08	6.45-7.89	7.41 ± 0.56
$[^1O_2^*]_{ss}$	4.92-13.47	7.58 ± 2.67	0.33-2.73	1.60 ± 0.90	0.16-3.14	1.15 ± 1.18	1.38-10.08	5.15 ± 3.52
$R_{f,^1O_2^*}$/[WSOC]	7.17-16.13	10.67±2.50	1.73-6.25	4.12±1.45	0.73-10.42	3.98±3.51	2.21-18.44	8.38±4.70
$\Phi_{^1O_2^*}$	3.49-8.78	5.92 ± 1.82	2.24-6.47	4.07 ± 1.40	1.19-9.54	4.36 ± 3.28	2.62-13.74	6.19 ± 3.22
$[^3C^*]_{ss}$	2.41-17.90	11.08 ± 6.50	0.35-15.80	6.44 ± 4.31	0.29-27.27	7.62 ± 9.47	2.97-80.77	17.72 ± 23.95
$R_{f,^3C^*}$/[WSOC]	1.14-7.25	4.62±2.42	0.48-8.74	4.73±2.39	0.42-24.93	6.65±8.16	2.08-43.54	9.84±12.98
$\Phi_{^3C^*}$	0.06-0.49	0.24 ± 0.13	0.07-1.44	0.50 ± 0.40	0.05-2.28	0.69 ± 0.74	0.14-3.24	0.80 ± 0.98

Note: The unit for each parameter is the same as in Table 1. Uncertainties are one standard deviation.

we used UVA light to illuminate the extracts in photochemical experiments, whereas previous studies used xenon arc lamps (Kaur et al., 2019) or a solar simulator instrument (Leresche et al., 2021). In addition, the different methodologies used to determine $\Phi_{^1O_2^*}$ may have contributed to our study's higher $\Phi_{^1O_2^*}$ values. While this study determined the $\Phi_{^1O_2^*}$ values from the $R_{f,^1O_2^*}$ and R_{abs} measurements (Equation 7), other studies used a reference $^1O_2^*$ sensitizer (e.g., perinaphthenone) to determine their $\Phi_{^1O_2^*}$ values (Manfrin et al., 2019; Bogler et al., 2022).

3.2.2 $^3C^*$

The pseudo first-order decay rate constants of syringol ($^3C^*$ chemical probe) in photochemical experiments (Figure S5) were used to determine the steady-state concentrations of $^3C^*$, $[^3C^*]_{ss}$ (Equation 8). The $[^3C^*]_{ss}$ values were close to the values calculated using only the bimolecular rate constant for the model $^3C^*$ species $^3DMB^*$ (Table S6). This indicated that the $^3C^*$ species quantified in this study had reactivities close to $^3DMB^*$. Similar observations were reported for $^3C^*$ species in PM extracts from biomass-influenced areas in California, USA (Kaur and Anastasio, 2018; Kaur et al., 2019). It is important to note that due to the chemical complexity of $^3C^*$ species, a single chemical probe cannot quantify all the $^3C^*$ species (Maizel and Remucal, 2017). Hence, only a subset of $^3C^*$ species that can oxidize syringol was quantified in our study (Kaur and Anastasio, 2018). The $[^3C^*]_{ss}$ values spanned two orders of magnitude, ranging from 2.93×10^{-16} to 8.08×10^{-14} M, with a study average of $(1.09 \pm 1.39) \times 10^{-14}$ M. While the range of $[^3C^*]_{ss}$ values was in line with those previously measured in atmospheric samples (10^{-16} to 10^{-12} M) (Table S7), not all of these previous studies used syringol as the $^3C^*$

chemical probe. The choice of the ^{3}C* chemical probe can impact the $[^3$C$^*]_{ss}$ measurements. This is because different ^{3}C* chemical probes react with different subsets of ^{3}C* species of different oxidizing abilities (Maizel and Remucal, 2017; Kaur and Anastasio, 2018; Ma et al., 2023c). In addition, the decays of oxidizing ^{3}C* chemical probes (e.g., syringol and 2,4,6-trimethylphenol) can be inhibited by the co-presence of some atmospheric species (e.g., copper, water-soluble organic matter), especially under highly concentrated conditions (Canonica and Laubscher, 2008; Maizel and Remucal, 2017; McCabe and Arnold, 2017; Ma et al., 2023b, c). Using the equations provided by Ma et al. (2023b), we estimate that our reported $[^3$C$^*]_{ss}$ values may be underestimated by as much as a factor of 2 due to water-soluble organic matter inhibiting the decay of syringol. In addition, water-soluble copper, another atmospheric species known to inhibit syringol decay (Ma et al., 2023c), can be present in substantial concentrations in PM$_{2.5}$ in some urban areas in Hong Kong (Yang et al., 2023). However, the extent to which water-soluble copper will impact $[^3$C$^*]_{ss}$ values is currently unknown. Nevertheless, the $[^3$C$^*]_{ss}$ values were linearly correlated with the WSOC concentration and α_{300} (Figures S11c and S11d), which was consistent with water-soluble BrC being a source of ^{3}C*. The correlations of $[^3$C$^*]_{ss}$ with the WSOC concentration and α_{300} were noticeably weaker than the correlations of $[^1$O$_2^*]_{ss}$ with the WSOC concentration and α_{300}. The weaker $[^3$C$^*]_{ss}$ correlations could be attributed to the chemical complexity of the ^{3}C* pool. Even though water-soluble BrC is a key precursor of ^{3}C*, the sample-to-sample variability in the subset of ^{3}C* species that were able to oxidize syringol likely caused the weaker $[^3$C$^*]_{ss}$ correlations with the WSOC concentration and α_{300}.

The formation rates of ^{3}C*, R$_{f,^3C^*}$, ranged from 2.20×10^{-10} to 6.68×10^{-8} M s^{-1}, with a study average of $(9.07 \pm 11.50) \times 10^{-9}$ M s^{-1} (Table S6). The study average WSOC-normalized R$_{f,^3C^*}$ $((6.51 \pm 7.90) \times 10^{-10}$ M s^{-1} L mg-C^{-1}) was 3 to 7 times lower than the previously reported value for PM samples collected in biomass burning-influenced areas in California, USA (Kaur et al., 2019; Ma et al., 2023a). Across all extracts, the R$_{f,^3C^*}$ was linearly correlated with R$_{abs}$, with a Pearson's r value of 0.63 (Figure S12b), which indicated that ^{3}C* production was linked to water-soluble BrC. The correlation between R$_{f,^3C^*}$ and R$_{abs}$ was weaker than the correlation between R$_{f,^1O_2^*}$ and R$_{abs}$. Kaur et al. (2019) similarly reported weaker linear correlations for R$_{abs}$ vs. R$_{f,^3C^*}$ compared to R$_{abs}$ vs. R$_{f,^1O_2^*}$ for extracts of winter PM collected from areas influenced by biomass burning emissions in California, USA. Sample-to-sample variability in the subset of ^{3}C* species that were able to oxidize syringol likely caused the weaker R$_{abs}$ vs. R$_{f,^3C^*}$ correlations.

The $\Phi_{^3C^*}$ values ranged from 0.05 to 3.24 %, with a study average of (0.55 ± 0.66) % which was approximately 9 times lower than the study average of $\Phi_{^1O_2^*}$. The difference in ^{3}C* and ^{1}O$_2^*$ photosensitization efficiencies could be due to only a subset of ^{3}C* species that can oxidize syringol being captured in our photochemical experiments since different ^{3}C* species may have different photosensitization efficiencies. Our study average $\Phi_{^3C^*}$ was also lower than the average $\Phi_{^3C^*}$ $((2.40 \pm 1.00)$ %) reported by Kaur et al. (2019) for extracts of PM collected from biomass burning-influenced areas in California, USA. This suggested that the water-soluble BrC in our extracts have a lower fraction of oxidizing ^{3}C* species compared to that in PM samples investigated by Kaur et al. (2019), which could be due to the different composition and age of water-soluble BrC in atmospheric PM.

3.3 Site and seasonal variations of $^1O_2^*$ and $^3C^*$ production

The steady-state concentrations and quantum yields of $^1O_2^*$ and $^3C^*$ were fairly similar among the three sites (Figures S13). Variations in these values across the three sites were not statistically significant ($p > 0.05$). This indicated that the location (i.e.,
390   urban vs. semi-rural) did not have a significant effect on the steady-state concentrations and photosensitization efficiencies of $^3C^*$ and $^1O_2^*$, which implied that water-soluble BrC from local $PM_{2.5}$ sources did not have a significant influence on the year-round $^3C^*$ and $^1O_2^*$ production. The large spreads in the steady-state concentration and quantum yield values highlighted the broad range of BrC chromophores present in the $PM_{2.5}$ at the three locations that are capable of photosensitizing $^1O_2^*$ and $^3C^*$.

395   Since the locations did not have a significant influence on the production of $^1O_2^*$ and $^3C^*$, we combined the $^1O_2^*$ and $^3C^*$ datasets from the three sites and separated them based on seasonality. We observed a distinct seasonal trend for $[^1O_2^*]_{ss}$ (Figure 4a). The $[^1O_2^*]_{ss}$ values were generally the highest in the winter, and the lowest in the summer (Table 2). The seasonal variations in the $[^1O_2^*]_{ss}$ were also found to be statistically significant ($p < 0.05$). The seasonal trend for $[^3C^*]_{ss}$ was noticeably weaker and was not statistically significant ($p > 0.05$) (Figure 4b). However, the $[^3C^*]_{ss}$ values were mostly higher in the fall and winter
400   and lower in the spring and summer (Table 2). The differences in the strengths of the seasonal trends of $[^1O_2^*]_{ss}$ (i.e., strong and statistically significant) and $[^3C^*]_{ss}$ (i.e., weak and statistically insignificant) could be attributed to sample-to-sample variations in $^3C^*$ species that can form $^1O_2^*$. Even though $^3C^*$ is a precursor of $^1O_2^*$, not all $^3C^*$ species will form $^1O_2^*$. In addition, high energy and strongly reducing $^3C^*$ species are not necessarily efficient $^1O_2^*$ photosensitizers (McNeill and Canonica, 2016). Sample-to-sample variability in the subset of $^3C^*$ species that were able to oxidize syringol could also have contributed to the
405   weak seasonal $[^3C^*]_{ss}$ trend. The fall $[^3C^*]_{ss}$ average (Table 2) was noticeably high, and this was due to the inclusion of an abnormally high $[^3C^*]_{ss}$ value ((8.08 ± 4.59) $\times 10^{-14}$ M) obtained for the HT271021 sample which was identified as a "far out outlier" by Tukey's fences. Unlike the other samples, we observed fast photobleaching for the HT271021 sample during the photochemical experiments (Figures S4 and S5), which likely resulted in over-estimated steady-state concentrations (Sections 2.4 and 2.5). It should be noted that while a high $[^1O_2^*]_{ss}$ value was also obtained for the HT271021 sample, it was not identified
410   as an outlier by Tukey's fences.

Overall, seasonality had noticeable effects on $[^1O_2^*]_{ss}$ and (to a lesser extent) $[^3C^*]_{ss}$, wherein these values were the highest in the fall and winter and the lowest in the summer. The seasonal trends of $[^1O_2^*]_{ss}$ and $[^3C^*]_{ss}$ correlated with the seasonal trends of the WSOC concentration and light absorption properties of water-soluble BrC (Figure S10). The fall and winter extracts had higher concentrations of and/or more absorbing water-soluble BrC comprised of organic matter of high aromaticity than the
415   spring and summer extracts. Thus, the higher concentrations of and/or more absorbing water-soluble BrC in the winter and fall extracts likely enhanced $^1O_2^*$ and $^3C^*$ production. In particular, additional statistical analyses (Student's t-tests) performed on the seasonal values for $[^1O_2^*]_{ss}$, $PM_{2.5}$ mass/H_2O mass ratio, WSOC concentration, and light absorption properties of water-soluble BrC (Table S8) suggested that the seasonal differences in the $[^1O_2^*]_{ss}$ values were driven primarily by the $PM_{2.5}$ mass concentration and WSOC concentration. Since the seasonal variations in $PM_{2.5}$ and water-soluble BrC were due to the seasonal

420 variations in long-range air mass transport, this implied that regional $PM_{2.5}$ sources located in continental areas north of Hong Kong contributed to the higher photooxidant production in the fall and winter.
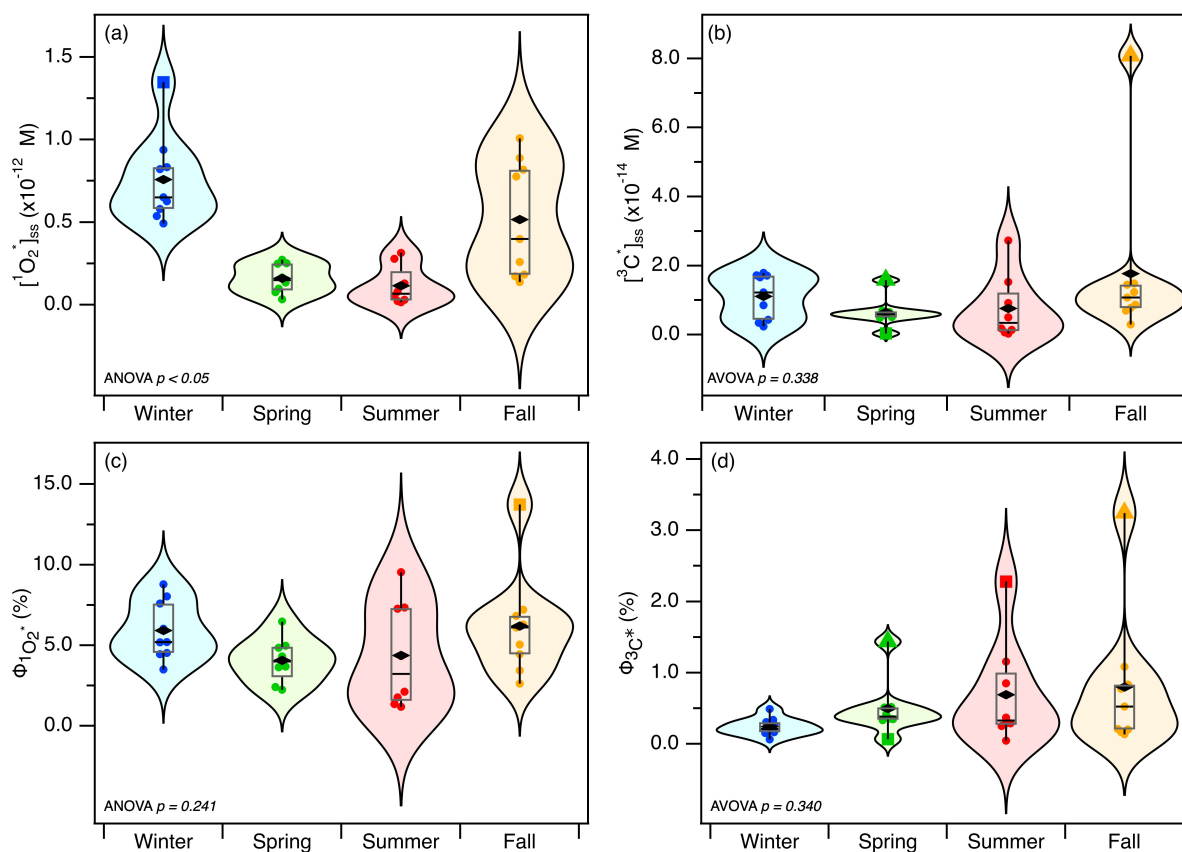
Figure 4. Violin plots showing the seasonal variations of (a) $[^1O_2^*]_{ss}$, (b) $[^3C^*]_{ss}$, (c) $\Phi_{^1O_2^*}$, and (d) $\Phi_{^3C^*}$. For the box plots, the squares indicate "far out outliers" and the triangles indicate outliers identified by Tukey's fences, the whiskers denote the minimum and maximum values, the boxes denote the 25th and 75th percentile values, black diamonds indicate the mean values, and the boxes' midline denote the median values.

The seasonal trends of $\Phi_{^1O_2^*}$ and $\Phi_{^3C^*}$ (Figures 4c and 4d) were noticeably weaker than the seasonal trends of $[^1O_2^*]_{ss}$ and $[^3C^*]_{ss}$ (Figures 4a and 4b). The average $\Phi_{^1O_2^*}$ for winter, spring, summer, and fall were (5.92 ± 1.82) %, (4.07 ± 1.40) %, (4.36 ± 3.28) %, and (6.19 ± 3.22) %, respectively, while the average $\Phi_{^3C^*}$ for winter, spring, summer, and fall were (0.24 ± 1.23) %, (0.50 ± 0.40) %, (0.69 ± 0.74) %, and (0.80 ± 0.98) %, respectively. The average $\Phi_{^1O_2^*}$ and $\Phi_{^3C^*}$ values were noticeably the highest for the fall season. This was due to the inclusion of abnormally high quantum yield values obtained for the HT271021 sample (identified as a "far out outlier" by Tukey's fences). Fast photobleaching for the HT271021 sample during the photochemical experiments (Figures S4 and S5) likely resulted in over-estimated quantum yields. The variations in

$\Phi_{^1O_2^*}$ and $\Phi_{^3C^*}$ across the four seasons were not statistically significant ($p > 0.05$), which indicated that seasonality did not have a significant effect on the photosensitization efficiencies of $^1O_2^*$ and $^3C^*$. However, we cannot discount the possibility that the statistically insignificant variations in $\Phi_{^1O_2^*}$ and $\Phi_{^3C^*}$ across the four seasons could be due to photobleaching. Leresche et al. (2021) previously reported reduced $^1O_2^*$ photosensitization for the extracts of summer $PM_{2.5}$ collected from Colorado, USA due to enhanced photobleaching. Thus, it is possible that the summer BrC chromophores may have been more effective in producing photooxidants but the enhanced photobleaching caused by stronger solar irradiation led to their weakened photosensitization ability and consequently resulted in statistically insignificant variations in $\Phi_{^1O_2^*}$ and $\Phi_{^3C^*}$ across the four seasons.

We also compared the influence of seasonal variations in long-range air mass transport on the $[^1O_2^*]_{ss}$ and $[^3C^*]_{ss}$ values for the urban CU and TW sites vs. semi-rural HT site. Since the spring sampling months could be viewed as a transition period wherein the dominant air masses that arrive in Hong Kong gradually shifted from the polluted continental northern areas (fall and winter months) to the clean marine southern regions (summer months) (Figures S6 to S8), for simplicity, we excluded the spring datatsets from this comparison. The fall and winter datatsets were combined and the subsequent average value was compared to the average value of the summer datatset. Larger contrasts in the $[^1O_2^*]_{ss}$ and $[^3C^*]_{ss}$ values were observed for the semi-rural HT site compared to the urban CU and TW sites (Tables S5 and S6), which were line with the larger contrasts in the average WSOC concentrations and light absorption properties for HT compared to CU and TW (Tables S2 and S3). This could be attributed to the nature of the sites. Due to the seasonal variations in long-range air mass transport (Figures S6 to S8), local sources are the main contributors to summer $PM_{2.5}$, whereas regional sources located in continental areas north of Hong Kong are the main contributors to fall and winter $PM_{2.5}$ (Pathak et al., 2003; Louie et al., 2005; Louie, 2005; Huang et al., 2014; Li et al., 2015; Wong et al., 2020). In contrast to the urban CU and TW sites, the semi-rural HT site is located far from urban areas (approximately 6 km away from the nearest urban area). Thus, contributions of local anthropogenic emissions (e.g., traffic, combustion-related activities) to water-soluble BrC in summer $PM_{2.5}$ at the semi-rural HT site are smaller compared to those at the urban CU and TW sites. This would result in larger contrasts between the average WSOC concentrations and light absorption properties from the combined fall + winter datatset vs. summer dataset for the semi-rural HT site compared to the urban CU and TW sites. Consequently, the higher concentrations of water-soluble BrC in summer $PM_{2.5}$ from local anthropogenic emissions at the urban CU and TW sites contributed to their higher summer $[^1O_2^*]_{ss}$ and $[^3C^*]_{ss}$ values, and consequently smaller fall + winter vs. summer $[^1O_2^*]_{ss}$ and $[^3C^*]_{ss}$ contrasts, compared to the semi-rural HT site.

3.4 Relating $[^3C^*]_{ss}$ and $[^1O_2^*]_{ss}$ to water-soluble BrC concentration and light absorption properties

To examine more closely how water-soluble BrC contributed to $^1O_2^*$ and $^3C^*$ production, we first investigated how the $[^1O_2^*]_{ss}$ and $[^3C^*]_{ss}$ values changed as a function of MAC_{300}, a light absorbance parameter that accounts for WSOC dilution. Both $[^1O_2^*]_{ss}$ and $[^3C^*]_{ss}$ showed positive correlations with MAC_{300} (Figures 5a and 5c), which indicated that the production of $^1O_2^*$ and $^3C^*$ were governed by the quantity and absorption efficiency of water-soluble BrC. $[^1O_2^*]_{ss}$ was noticeably more strongly linearly correlated with MAC_{300} compared to $[^3C^*]_{ss}$. The weaker $[^3C^*]_{ss}$ correlations could be attributed to the chemical complexity of the $^3C^*$ pool which cannot be quantified completely by syringol. Thus, even though water-soluble BrC is a

key precursor of $^3C^*$, the sample-to-sample variability in the size of the population of $^3C^*$ species that were able to oxidize syringol likely caused the weaker $[^3C^*]_{ss}$ correlations with MAC_{300}.
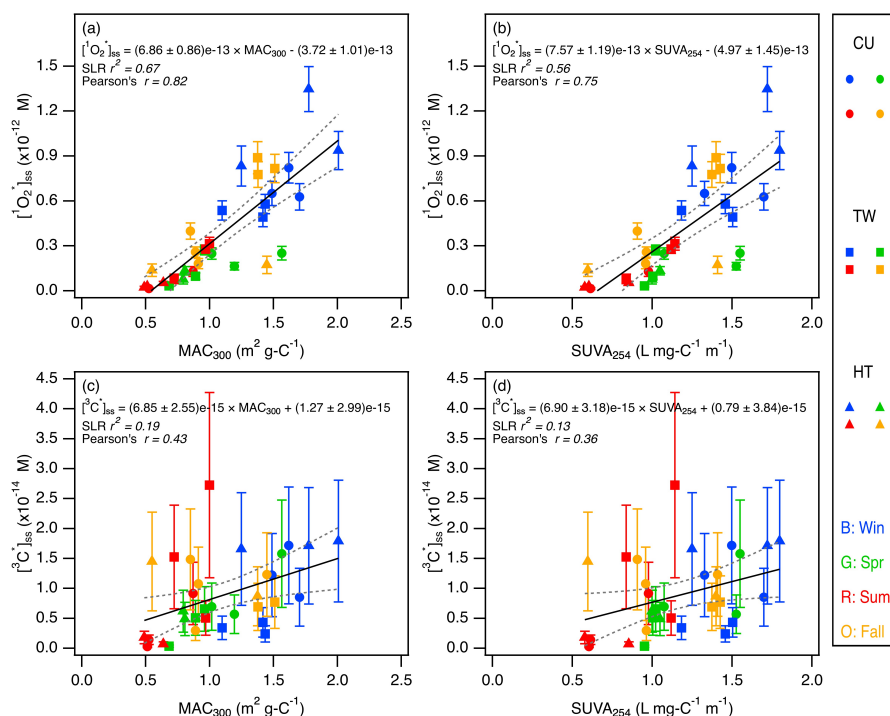
Figure 5. (a and b) $[^1O_2^*]_{ss}$ and (c and d) $[^3C^*]_{ss}$ as a function of MAC_{300} and $SUVA_{254}$. The outlier, HT271021, was excluded. Blue, green, red, and orange symbols denote the winter, spring, summer, and fall samples, respectively. Dashed lines represent 95 % confidence bands. SLR r^2 and Pearson's r indicate coefficient of determination of simple linear regression and Pearson correlation coefficient, respectively.

The $[^1O_2^*]_{ss}$ and $[^3C^*]_{ss}$ depend on both the quality and quantity of the BrC chromophores. The quantity of the BrC chro-
465 mophores is associated with their concentrations, whereas the quality is associated with their quantum yields and WSOC-normalized light absorption properties (e.g., MAC and SUVA values) (Bogler et al., 2022). In other words, some BrC chromophores are more efficient as making photooxidants, and thus $PM_{2.5}$ with higher quantum yields can be considered to have higher quality BrC chromophores towards $^1O_2^*$ and $^3C^*$ formation. A high WSOC concentration in an extract will result in a high $[^1O_2^*]_{ss}$ (and/or a high $[^3C^*]_{ss}$) only if a high concentration of water-soluble BrC chromophores is present in the extract.
470 The relative importance in the quantity vs. quality of BrC chromophores in our study could be ascertained from the comparison of the seasonal trends of $[^1O_2^*]_{ss}$ and $[^3C^*]_{ss}$ (Figures 4a and 4b) vs. the seasonal trends of $\Phi_{^1O_2^*}$ and $\Phi_{^3C^*}$ (Figures 4c and 4d). Stronger seasonal trends were observed for $[^1O_2^*]_{ss}$ and $[^3C^*]_{ss}$, which indicated that the quantity of BrC chromophores mainly governed $^1O_2^*$ and $^3C^*$ production in our study. The important role that the quantity of BrC chromophores plays in driving $^1O_2^*$ and $^3C^*$ production is further emphasized by the weakened seasonal trends of WSOC-normalized $[^1O_2^*]_{ss}$ and $[^3C^*]_{ss}$ values
475 (Section S3 and Figure S14).

Even though the quantity of BrC chromophores appeared to be the main driver of $^1O_2^*$ and $^3C^*$ production in our study, it is still worth investigating factors that affected the quality of BrC chromophores. We hypothesized that the quality of BrC chromophores was influenced by the presence of light absorbing aromatic compounds (Laskin et al., 2015). To test this hypothesis, we evaluated the contributions of aromatic compounds to $^1O_2^*$ and $^3C^*$ production by plotting the $[^1O_2^*]_{ss}$ and $[^3C^*]_{ss}$ values as a function of two commonly used indicators of aromaticity, SUVA$_{254}$ and SUVA$_{365}$ (Figures 5b, 5d, and S15). Both $[^1O_2^*]_{ss}$ and $[^3C^*]_{ss}$ generally showed positive correlations with SUVA$_{254}$ and SUVA$_{365}$. These correlations provided evidence that the production of $^1O_2^*$ and $^3C^*$ was enhanced by aromatic compounds. This enhancement likely occurred though a combination of enhanced rates of light absorption and photosensitization of water-soluble BrC chromophores (Manfrin et al., 2019; Chen et al., 2021). The linear correlations of $[^3C^*]_{ss}$ with SUVA$_{254}$ and SUVA$_{365}$ were noticeably weaker compared to $[^1O_2^*]_{ss}$. The weaker $[^3C^*]_{ss}$ correlations could be attributed to the sample-to-sample variability in the size of the population of $^3C^*$ species that were able to oxidize syringol.

It is important to note that even though our results (Figures 5b, 5d, and S15) indicated that aromatic compounds were likely key water-soluble BrC constituents and photosensitizers that enhanced $^1O_2^*$ and $^3C^*$ production, there are other water-soluble BrC constituents and photosensitizers that can also promote $^1O_2^*$ and $^3C^*$ production. One such example are imidazoles, which are formed from aqueous reactions of dicarbonyls with reduced nitrogen-containing compounds such as amines, ammonium ions, and amino acids (Haan et al., 2009; De Haan et al., 2009, 2011; Kampf et al., 2012; Powelson et al., 2014). Recent studies have shown that imidazoles can also be formed from aqueous $^3C^*$ -photosensitized reactions of phenolic compounds in the presence of ammonium ions (Mabato et al., 2022, 2023). To the best of our knowledge, there has not been a study that have investigated the concentrations of imidazoles in atmospheric PM in Hong Kong. However, imidazoles have been detected in atmospheric PM in urban Guangzhou (another city in South China) (Lian et al., 2022) and at a background forest site in the Nanling Mountains of South China (He et al., 2022). Thus, future studies can focus on identifying other water-soluble BrC constituents and photosensitizers (e.g., imidazoles) in atmospheric PM in Hong Kong that can play potentially important roles in enhancing $^1O_2^*$ and $^3C^*$ production.

4 Conclusions and implications

In this study, we reported the steady-state concentrations and quantum yields of $^3C^*$ and $^1O_2^*$ produced by PM$_{2.5}$ in Hong Kong, South China. We quantified the production of $^3C^*$ and $^1O_2^*$ in illuminated aqueous extracts of PM$_{2.5}$ collected in different seasons at two urban sites and one coastal semi-rural site during a year-round study. Variations in the WSOC concentrations and light absorption properties of water-soluble BrC across the three sites were found to be statistically insignificant. In contrast, variations in the WSOC concentrations and light absorption properties of water-soluble BrC across the four seasons were significant. Higher concentrations of WSOC and more light absorbing water-soluble BrC were present in the the PM$_{2.5}$ during the fall and winter months. This could be attributed to monsoon-influenced seasonal variations in long-range air mass transport to Hong Kong. Air masses originating mainly from polluted continental areas located north of Hong Kong contributed to the higher concentrations of WSOC and more light absorbing water-soluble BrC in the the fall and winter PM$_{2.5}$, whereas air

masses originating mainly from clean marine regions located south of Hong Kong were responsible for the lower concentrations of WSOC and less light absorbing water-soluble BrC in the summer $PM_{2.5}$.

$^1O_2^*$ and $^3C^*$ were produced in all the illuminated aqueous extracts of $PM_{2.5}$. The $[^1O_2^*]_{ss}$ spanned two orders of magnitude, ranging from 1.56×10^{-14} to 1.35×10^{-12} M, with a study average of $(4.02 \pm 3.52) \times 10^{-13}$ M. The $[^3C^*]_{ss}$ spanned two orders of magnitude, ranging from 2.93×10^{-16} to 8.08×10^{-14} M, with a study average of $(1.09 \pm 1.39) \times 10^{-14}$ M. These $[^1O_2^*]_{ss}$ and $[^3C^*]_{ss}$ values were in line with the steady-state concentrations previously reported for PM extracts, fog water, and rain water (Table S7). The $[^1O_2^*]_{ss}$ and $[^3C^*]_{ss}$ correlated with the concentration of WSOC and the absorbance of water-soluble BrC, which indicated that water-soluble BrC was a key source of $^1O_2^*$ and $^3C^*$. Positive linear correlations between their steady-state concentrations and indicators of aromaticity ($SUVA_{254}$ and $SUVA_{365}$) implied that the production of $^1O_2^*$ and $^3C^*$ was enhanced by aromatic compounds, likely though a combination of enhanced rates of light absorption and photosensitization of water-soluble BrC chromophores. Location (i.e., urban vs. semi-rural) did not have a significant effect on $[^1O_2^*]_{ss}$ and $[^3C^*]_{ss}$, which indicated that BrC from local $PM_{2.5}$ sources were likely not the primary drivers of year-round $^3C^*$ and $^1O_2^*$ production. In contrast, seasonality had a significant effect on $[^1O_2^*]_{ss}$ and $[^3C^*]_{ss}$, with higher $[^1O_2^*]_{ss}$ and $[^3C^*]_{ss}$ observed in the fall and winter compared to the summer. This indicated that the seasonal trends of $^1O_2^*$ and $^3C^*$ production in $PM_{2.5}$ in Hong Kong were governed by the seasonal variations in long-range air mass transport. Consequently, regional $PM_{2.5}$ sources located in continental areas north of Hong Kong contributed to the higher $^1O_2^*$ and $^3C^*$ production in the fall and winter.

Even though the steady-state concentrations of ·OH ($[·OH]_{ss}$) were not measured in this study due to insufficient extract volumes, previous studies have reported that they are typically on the order of 10^{-17} to 10^{-15} M (Arakaki and Faust, 1998; Arakaki et al., 1999, 2006, 2013; Anastasio and McGregor, 2001; Anastasio and Jordan, 2004; Anastasio and Newberg, 2007; Kaur and Anastasio, 2017; Kaur et al., 2019; Manfrin et al., 2019). We hypothesize that the $[·OH]_{ss}$ in our illuminated extracts are also on the order of 10^{-17} to 10^{-15} M. The main precursors of ·OH in Hong Kong are likely BrC and inorganic nitrate, both of which have the highest concentrations in the winter and the lowest concentrations in the summer (Table S2). Therefore, it is likely that ·OH production will have a similar seasonal trend as $^3C^*$ and $^1O_2^*$ production. Consequently, the concentrations of $^3C^*$ and $^1O_2^*$ can potentially be up to 10^3 and 10^5 higher than than the concentrations of ·OH in the extracts, respectively. Based on work by Kaur et al. (2019) and Ma et al. (2023b), the differences between the $^3C^*$ and $^1O_2^*$ concentrations vs. ·OH concentrations are expected to be even larger under aerosol liquid water conditions. Thus, despite the lower reactivities of organic aerosol compounds with $^1O_2^*$ and $^3C^*$ compared to their corresponding reactvities with ·OH, $^1O_2^*$ and $^3C^*$ will likely be present at high enough concentrations that they can be competitive photooxidants to ·OH under aerosol liquid water conditions (Kaur et al., 2019; Manfrin et al., 2019). This necessitates the inclusion of aqueous reactions involving $^1O_2^*$ and $^3C^*$ with organic aerosol compounds into atmospheric models since these photooxidants may play important roles in the photochemical processing of organic aerosol compounds in atmospheric aqueous phases due to their high concentrations offsetting their lower reactivities.

The significance of our results lies foremost in the seasonal trends observed for $[^1O_2^*]_{ss}$ and $[^3C^*]_{ss}$, and how they correlated with the seasonal variations in the long-range air mass transport. Since many South China cities share similar monsoon-

influenced seasonal air quality and aerosol pollution characteristics as Hong Kong, we anticipate that many South China cities will have similar seasonal trends of $^1O_2^*$ and $^3C^*$ production in atmospheric aerosols. In addition, given that their high concentrations will likely offset their lower reactivities, $^1O_2^*$ and $^3C^*$ seasonality in atmospheric aerosols can potentially influence the aqueous photochemical processing of organic aerosol compounds in South China, a region in which aqueous aerosol chemistry plays important roles in the formation and transformation of SOA (Li et al., 2013b, a). It should be noted that although our results showed that the location (i.e., urban vs. semi-rural) did not have a significant effect on $^1O_2^*$ and $^3C^*$ production in $PM_{2.5}$ in Hong Kong, this may not necessarily be the case for other South China cities, especially those that are located close to areas with biomass burning activities (Yuan et al., 2015).

While this study reports the first measurements of the quantum yields and steady-state concentrations of $^3C^*$ and $^1O_2^*$ produced in atmospheric aerosols in South China, there are a number of caveats that should be noted. First, the $[^1O_2^*]_{ss}$ and $[^3C^*]_{ss}$ values reported in our study serve as lower limits since they were measured using extracts comprised of only the water-soluble fraction of $PM_{2.5}$. Water-insoluble BrC, which reportedly dominates the total BrC absorption in some parts of China (Bai et al., 2020; Huang et al., 2020; Wang et al., 2022), will likely produce $^1O_2^*$ and $^3C^*$ as well. Second, due to limited extract volumes for photochemical experiments and chemical analysis, only one $^3C^*$ chemical probe was used in our study to quantify $^3C^*$ quantum yields, formation rates, and steady-state concentrations. Hence, we only report concentrations of a subset of $^3C^*$ species. Measurements of $^3C^*$ quantum yields and steady-state concentrations can be better constrained with the use of multiple $^3C^*$ probes (Kaur and Anastasio, 2018; Kaur et al., 2019; Ma et al., 2023b, c). Third, photochemical experiments were performed using diluted extracts. These experimental conditions were substantially more diluted than atmospheric $PM_{2.5}$ conditions. Thus, the concentrations of BrC chromophores in our extracts were substantially lower than those in atmospheric $PM_{2.5}$, which would influence the reaction kinetics, and consequently $^3C^*$ and $^1O_2^*$ production. Based on work by Kaur et al. (2019) and Ma et al. (2023b), higher $[^1O_2^*]_{ss}$ and $[^3C^*]_{ss}$ in atmospheric $PM_{2.5}$ are expected due to the higher concentrations of BrC chromophores, though extrapolation from dilute extract conditions to concentrated $PM_{2.5}$ conditions is complex and non-linear. Fourth, our extracts were not buffered and their average pH was 4.68 ± 0.29, whereas the pH of atmospheric $PM_{2.5}$ in Hong Kong has been reported to be between 1.8 and 5.1 (Nah and Lam, 2022; Nah et al., 2023). pH can influence the composition of protonated vs. unprotonated BrC chromophores, which in turn will affect their absorption and reaction kinetics (Ma et al., 2021). Fifth, this work focuses on $^1O_2^*$ and $^3C^*$ production in $PM_{2.5}$ extracts. Previous work on $^1O_2^*$ production in illuminated extracts of size-fractionated supermicron-sized road dust (< 45 to 500 µm) suggest that aerosol size may influence $^1O_2^*$ production (Cote et al., 2018). At present, it is unclear how aerosol size within atmospheric $PM_{2.5}$ influences $^1O_2^*$ and $^3C^*$ production. Hence, the effects of dilution, pH, and aerosol size on photooxidant production from both water-soluble and water-insoluble BrC in atmospheric PM should be explored in future studies to further our understanding of aqueous organic aerosol photochemistry in the South China region.

Data availability. Light absorption and kinetic data have been submitted to the data repository Zenodo (https://doi.org/10.5281/zenodo.7827983). Data can also be made available upon request to the corresponding author (theodora.nah@cityu.edu.hk).

Author contributions. YLyu and TN designed the study. YHL collected the field samples. YLyu performed the chemical analysis and experiments. YLyu, YLi, NBD, and TN analyzed the data. YLyu and TN prepared the manuscript with contributions from all co-authors.

Competing interests. One of the authors is a member of the editorial board of *Atmospheric Chemistry and Physics*. The peer-review process
580   was guided by an independent editor, and the authors also have no other competing interests to declare.

Acknowledgements. We acknowledge the assistance of Yanhao Miao with the backward trajectory analysis, Jason Lam for his assistance with the furfuryl alcohol distillation, Wing Chi Au and Chung Ming Tai for their help on filter extraction and/or chemical analysis. The work described in this paper was supported by a grant from the Research Grants Council of the Hong Kong Special Administrative Region, China (Project No. 11303720).

References

Albinet, A., Minero, C., and Vione, D.: Photochemical generation of reactive species upon irradiation of rainwater: Negligible photoactivity of dissolved organic matter, Science of the total environment, 408, 3367–3373, 2010.

Allen, J. M., Gossett, C. J., and Allen, S. K.: Photochemical formation of singlet molecular oxygen (1O2) in illuminated aqueous solutions of p-aminobenzoic acid (PABA), Journal of Photochemistry and Photobiology B: Biology, 32, 33–37, https://doi.org/10.1016/1011-1344(95)07185-7, 1996.

Anastasio, C. and Jordan, A. L.: Photoformation of hydroxyl radical and hydrogen peroxide in aerosol particles from Alert, Nunavut: implications for aerosol and snowpack chemistry in the Arctic, Atmospheric Environment, 38, 1153–1166, https://doi.org/10.1016/j.atmosenv.2003.11.016, 2004.

Anastasio, C. and McGregor, K. G.: Chemistry of fog waters in California's Central Valley: 1. In situ photoformation of hydroxyl radical and singlet molecular oxygen, Atmospheric Environment, 35, 1079–1089, 2001.

Anastasio, C. and Newberg, J. T.: Sources and sinks of hydroxyl radical in sea-salt particles, Journal of Geophysical Research: Atmospheres, 112, https://doi.org/10.1029/2006JD008061, 2007.

Appiani, E., Ossola, R., Latch, D. E., Erickson, P. R., and McNeill, K.: Aqueous singlet oxygen reaction kinetics of furfuryl alcohol: effect of temperature, pH, and salt content, Environmental Science: Processes & Impacts, 19, 507–516, https://doi.org/10.1039/C6EM00646A, 2017.

Arakaki, T. and Faust, B. C.: Sources, sinks, and mechanisms of hydroxyl radical (• OH) photoproduction and consumption in authentic acidic continental cloud waters from Whiteface Mountain, New York: The role of the Fe (r)(r= II, III) photochemical cycle, Journal of Geophysical Research: Atmospheres, 103, 3487–3504, https://doi.org/10.1029/97JD02795, 1998.

Arakaki, T., Miyake, T., Shibata, M., and Sakugawa, H.: Photochemical formation and scavenging of hydroxyl radical in rain and dew waters, Nippon Kagaku Kaishi, pp. 335–340, https://doi.org/10.14934/chikyukagaku.43.15, 1999.

Arakaki, T., Kuroki, Y., Okada, K., Nakama, Y., Ikota, H., Kinjo, M., Higuchi, T., Uehara, M., and Tanahara, A.: Chemical composition and photochemical formation of hydroxyl radicals in aqueous extracts of aerosol particles collected in Okinawa, Japan, Atmospheric Environment, 40, 4764–4774, https://doi.org/10.1016/j.atmosenv.2006.04.035, 2006.

Arakaki, T., Anastasio, C., Kuroki, Y., Nakajima, H., Okada, K., Kotani, Y., Handa, D., Azechi, S., Kimura, T., Tsuhako, A., et al.: A general scavenging rate constant for reaction of hydroxyl radical with organic carbon in atmospheric waters, Environmental science & technology, 47, 8196–8203, https://doi.org/10.1021/es401927b, 2013.

Bai, Z., Zhang, L., Cheng, Y., Zhang, W., Mao, J., Chen, H., Li, L., Wang, L., and Chen, J.: Water/Methanol-Insoluble Brown Carbon Can Dominate Aerosol-Enhanced Light Absorption in Port Cities, Environmental Science & Technology, 54, 14 889–14 898, https://doi.org/10.1021/acs.est.0c03844, pMID: 32790286, 2020.

Barrios, B., Mohrhardt, B., Doskey, P. V., and Minakata, D.: Mechanistic insight into the reactivities of aqueous-phase singlet oxygen with organic compounds, Environmental Science & Technology, 55, 8054–8067, https://doi.org/10.1021/acs.est.1c01712, 2021.

Bilal, M., Nichol, J. E., Nazeer, M., Shi, Y., Wang, L., Kumar, K. R., Ho, H. C., Mazhar, U., Bleiweiss, M. P., Qiu, Z., et al.: Characteristics of fine particulate matter (PM2. 5) over urban, suburban, and rural areas of Hong Kong, Atmosphere, 10, 496, https://doi.org/10.3390/atmos10090496, 2019.

620   Bogler, S., Daellenbach, K. R., Bell, D. M., Prévôt, A. S., El Haddad, I., and Borduas-Dedekind, N.: Singlet Oxygen Seasonality in Aqueous PM10 is Driven by Biomass Burning and Anthropogenic Secondary Organic Aerosol, Environmental Science & Technology, 56, 15 389–15 397, https://doi.org/10.1021/acs.est.2c04554, 2022.

Canonica, S. and Laubscher, H.-U.: Inhibitory effect of dissolved organic matter on triplet-induced oxidation of aquatic contaminants, Photochemical & Photobiological Sciences, 7, 547–551, https://doi.org/10.1039/b719982a, 2008.

625   Canonica, S., Jans, U., Stemmler, K., and Hoigne, J.: Transformation kinetics of phenols in water: photosensitization by dissolved natural organic material and aromatic ketones, Environmental science & technology, 29, 1822–1831, https://doi.org/10.1021/es00007a020, 1995.

Canonica, S., Hellrung, B., and Wirz, J.: Oxidation of phenols by triplet aromatic ketones in aqueous solution, The Journal of Physical Chemistry A, 104, 1226–1232, https://doi.org/10.1021/jp9930550, 2000.

Chen, J., Li, C., Ristovski, Z., Milic, A., Gu, Y., Islam, M. S., Wang, S., Hao, J., Zhang, H., He, C., Guo, H., Fu, H., Milje-

630   vic, B., Morawska, L., Thai, P., LAM, Y. F., Pereira, G., Ding, A., Huang, X., and Dumka, U. C.: A review of biomass burning: Emissions and impacts on air quality, health and climate in China, Science of The Total Environment, 579, 1000–1034, https://doi.org/https://doi.org/10.1016/j.scitotenv.2016.11.025, 2017.

Chen, Q., Mu, Z., Xu, L., Wang, M., Wang, J., Shan, M., Fan, X., Song, J., Wang, Y., Lin, P., et al.: Triplet-state organic matter in atmospheric aerosols: Formation characteristics and potential effects on aerosol aging, Atmospheric Environment, 252, 118 343,

635   https://doi.org/10.1016/j.atmosenv.2021.118343, 2021.

Chen, X. and Yu, J. Z.: Measurement of organic mass to organic carbon ratio in ambient aerosol samples using a gravimetric technique in combination with chemical analysis, Atmospheric Environment, 41, 8857–8864, 2007.

Chow, W. S., Liao, K., Huang, X., Leung, K. F., Lau, A. K., and Yu, J. Z.: Measurement report: The 10-year trend of PM 2.5 major components and source tracers from 2008 to 2017 in an urban site of Hong Kong, China, Atmospheric Chemistry and Physics, 22, 11 557–11 577,

640   https://doi.org/10.5194/acp-22-11557-2022, 2022.

Cote, C. D., Schneider, S. R., Lyu, M., Gao, S., Gan, L., Holod, A. J., Chou, T. H., and Styler, S. A.: Photochemical production of singlet oxygen by urban road dust, Environmental Science & Technology Letters, 5, 92–97, https://doi.org/10.1021/acs.estlett.7b00533, 2018.

Cui, L., Wang, X. L., Ho, K. F., Gao, Y., Liu, C., Ho, S. S. H., Li, H. W., Lee, S. C., Wang, X. M., Jiang, B. Q., et al.: Decrease of VOC emissions from vehicular emissions in Hong Kong from 2003 to 2015: Results from a tunnel study, Atmospheric Environment, 177,

645   64–74, https://doi.org/10.1016/j.atmosenv.2018.01.020, 2018.

Davis, C. A., McNeill, K., and Janssen, E. M.-L.: Non-singlet oxygen kinetic solvent isotope effects in aquatic photochemistry, Environmental science & technology, 52, 9908–9916, https://doi.org/10.1021/acs.est.8b01512, 2018.

De Haan, D. O., Tolbert, M. A., and Jimenez, J. L.: Atmospheric condensed-phase reactions of glyoxal with methylamine, Geophysical Research Letters, 36, https://doi.org/https://doi.org/10.1029/2009GL037441, 2009.

650   De Haan, D. O., Hawkins, L. N., Kononenko, J. A., Turley, J. J., Corrigan, A. L., Tolbert, M. A., and Jimenez, J. L.: Formation of Nitrogen-Containing Oligomers by Methylglyoxal and Amines in Simulated Evaporating Cloud Droplets, Environmental Science & Technology, 45, 984–991, https://doi.org/10.1021/es102933x, pMID: 21171623, 2011.

Du, Z., He, K., Cheng, Y., Duan, F., Ma, Y., Liu, J., Zhang, X., Zheng, M., and Weber, R.: A yearlong study of water-soluble organic carbon in Beijing II: Light absorption properties, Atmospheric Environment, 89, 235–241, https://doi.org/10.1016/j.atmosenv.2014.02.022, 2014.

655   Erickson, P. R., Walpen, N., Guerard, J. J., Eustis, S. N., Arey, J. S., and McNeill, K.: Controlling factors in the rates of oxidation of anilines and phenols by triplet methylene blue in aqueous solution, The Journal of Physical Chemistry A, 119, 3233–3243, https://doi.org/10.1021/jp511408f, 2015.

Faust, B. C. and Allen, J. M.: Aqueous-phase photochemical sources of peroxyl radicals and singlet molecular oxygen in clouds and fog, Journal of Geophysical Research: Atmospheres, 97, 12 913–12 926, https://doi.org/10.1029/92JD00843, 1992.

660 Ghogare, A. A. and Greer, A.: Using singlet oxygen to synthesize natural products and drugs, Chemical reviews, 116, 9994–10 034, 2016.

Guo, H., Lee, S., Ho, K., Wang, X., and Zou, S.: Particle-associated polycyclic aromatic hydrocarbons in urban air of Hong Kong, Atmospheric Environment, 37, 5307–5317, https://doi.org/10.1016/j.atmosenv.2003.09.011, 2003.

Haag, W. R. and Hoigne, J.: Singlet oxygen in surface waters. 3. Photochemical formation and steady-state concentrations in various types of waters, Environmental science & technology, 20, 341–348, 1986.

665 Haan, D. O. D., Corrigan, A. L., Smith, K. W., Stroik, D. R., Turley, J. J., Lee, F. E., Tolbert, M. A., Jimenez, J. L., Cordova, K. E., and Ferrell, G. R.: Secondary Organic Aerosol-Forming Reactions of Glyoxal with Amino Acids, Environmental Science & Technology, 43, 2818–2824, https://doi.org/10.1021/es803534f, pMID: 19475956, 2009.

He, C., Wang, H., Gong, D., Lv, S., Wu, G., Wang, R., Chen, Y., Ding, Y., Li, Y., and Wang, B.: Insights into high concentrations of particle-bound imidazoles in the background atmosphere of southern China: Potential sources and influencing factors, Science of The
670 Total Environment, 806, 150 804, https://doi.org/https://doi.org/10.1016/j.scitotenv.2021.150804, 2022.

Helin, A., Virkkula, A., Backman, J., Pirjola, L., Sippula, O., Aakko-Saksa, P., Väätäinen, S., Mylläri, F., Järvinen, A., Bloss, M., et al.: Variation of absorption Ångström exponent in aerosols from different emission sources, Journal of Geophysical Research: Atmospheres, 126, e2020JD034 094, https://doi.org/10.1029/2020JD034094, 2021.

Hems, R. F., Schnitzler, E. G., Liu-Kang, C., Cappa, C. D., and Abbatt, J. P.: Aging of atmospheric brown carbon aerosol, ACS Earth and
675 Space Chemistry, 5, 722–748, https://doi.org/10.1021/acsearthspacechem.0c00346, 2021.

Herckes, P., Valsaraj, K. T., and Collett Jr, J. L.: A review of observations of organic matter in fogs and clouds: Origin, processing and fate, Atmospheric research, 132, 434–449, https://doi.org/10.1016/j.atmosres.2013.06.005, 2013.

Herrmann, H., Schaefer, T., Tilgner, A., Styler, S. A., Weller, C., Teich, M., and Otto, T.: Tropospheric aqueous-phase chemistry: kinetics, mechanisms, and its coupling to a changing gas phase, Chemical reviews, 115, 4259–4334, https://doi.org/10.1021/cr500447k, 2015.

680 Herzberg, L. and Herzberg, G.: Fine Structure of the Infrared Atmospheric Oxygen Bands., The Astrophysical Journal, 105, 353, https://doi.org/10.1086/144910, 1947.

Huang, R.-J., Yang, L., Shen, J., Yuan, W., Gong, Y., Guo, J., Cao, W., Duan, J., Ni, H., Zhu, C., Dai, W., Li, Y., Chen, Y., Chen, Q., Wu, Y., Zhang, R., Dusek, U., O'Dowd, C., and Hoffmann, T.: Water-Insoluble Organics Dominate Brown Carbon in Wintertime Urban Aerosol of China: Chemical Characteristics and Optical Properties, Environmental Science & Technology, 54, 7836–7847,
685 https://doi.org/10.1021/acs.est.0c01149, pMID: 32479722, 2020.

Huang, X. H., Bian, Q., Ng, W. M., Louie, P. K., Yu, J. Z., et al.: Characterization of PM2. 5 major components and source investigation in suburban Hong Kong: a one year monitoring study, Aerosol and Air Quality Research, 14, 237–250, https://doi.org/10.4209/aaqr.2013.01.0020, 2014.

Kampf, C. J., Jakob, R., and Hoffmann, T.: Identification and characterization of aging products in the glyoxal/ammonium sul-
690 fate system–implications for light-absorbing material in atmospheric aerosols, Atmospheric Chemistry and Physics, 12, 6323–6333, https://doi.org/10.5194/acp-12-6323-2012, 2012.

Kaur, R. and Anastasio, C.: Light absorption and the photoformation of hydroxyl radical and singlet oxygen in fog waters, Atmospheric Environment, 164, 387–397, https://doi.org/10.1016/j.atmosenv.2017.06.006, 2017.

Kaur, R. and Anastasio, C.: First measurements of organic triplet excited states in atmospheric waters, Environmental science & technology,
695 52, 5218–5226, https://doi.org/10.1021/acs.est.7b06699, 2018.

Kaur, R., Labins, J. R., Helbock, S. S., Jiang, W., Bein, K. J., Zhang, Q., and Anastasio, C.: Photooxidants from brown carbon and other chromophores in illuminated particle extracts, Atmospheric Chemistry and Physics, 19, 6579–6594, https://doi.org/10.5194/acp-19-6579-2019, 2019.

Kirchstetter, T. W., Novakov, T., and Hobbs, P. V.: Evidence that the spectral dependence of light absorption by aerosols is affected by organic carbon, Journal of Geophysical Research: Atmospheres, 109, https://doi.org/10.1029/2004JD004999, 2004.

Laskin, A., Laskin, J., and Nizkorodov, S. A.: Chemistry of atmospheric brown carbon, Chemical reviews, 115, 4335–4382, https://doi.org/10.1021/cr5006167, 2015.

Lathioor, E. C. and Leigh, W. J.: Bimolecular hydrogen abstraction from phenols by aromatic ketone triplets, Photochemistry and photobiology, 82, 291–300, https://doi.org/10.1562/2005-06-20-RA-581, 2006.

Leresche, F., McKay, G., Kurtz, T., von Gunten, U., Canonica, S., and Rosario-Ortiz, F. L.: Effects of Ozone on the Photochemical and Photophysical Properties of Dissolved Organic Matter, Environmental Science & Technology, 53, 5622–5632, https://doi.org/10.1021/acs.est.8b06410, pMID: 31022348, 2019.

Leresche, F., Salazar, J. R., Pfotenhauer, D. J., Hannigan, M. P., Majestic, B. J., and Rosario-Ortiz, F. L.: Photochemical aging of atmospheric particulate matter in the aqueous phase, Environmental Science & Technology, 55, 13 152–13 163, https://doi.org/10.1021/acs.est.1c00978, 2021.

Li, J., Chen, Q., and Guan, D.: Insights into the triplet photochemistry of atmospheric aerosol and subfractions isolated with different polarity, Atmospheric Environment, 290, 119 375, 2022.

Li, N., Fu, T.-M., Cao, J., Lee, S., Huang, X.-F., He, L.-Y., Ho, K.-F., Fu, J. S., and Lam, Y.-F.: Sources of secondary organic aerosols in the Pearl River Delta region in fall: Contributions from the aqueous reactive uptake of dicarbonyls, Atmospheric Environment, 76, 200–207, https://doi.org/https://doi.org/10.1016/j.atmosenv.2012.12.005, improving Regional Air Quality over the Pearl River Delta and Hong Kong: from Science to Policy, 2013a.

Li, Y., Lee, B. P., Su, L., Fung, J. C. H., and Chan, C. K.: Seasonal characteristics of fine particulate matter (PM) based on high-resolution time-of-flight aerosol mass spectrometric (HR-ToF-AMS) measurements at the HKUST Supersite in Hong Kong, Atmospheric Chemistry and Physics, 15, 37–53, 2015.

Li, Y. J., Lee, B. Y. L., Yu, J. Z., Ng, N. L., and Chan, C. K.: Evaluating the degree of oxygenation of organic aerosol during foggy and hazy days in Hong Kong using high-resolution time-of-flight aerosol mass spectrometry (HR-ToF-AMS), Atmospheric Chemistry and Physics, 13, 8739–8753, https://doi.org/10.5194/acp-13-8739-2013, 2013b.

Li, Z., Xue, L., Yang, X., Zha, Q., Tham, Y. J., Yan, C., Louie, P. K., Luk, C. W., Wang, T., and Wang, W.: Oxidizing capacity of the rural atmosphere in Hong Kong, Southern China, Science of the total environment, 612, 1114–1122, https://doi.org/10.1016/j.scitotenv.2017.08.310, 2018.

Lian, X., Tang, G., Dao, X., Hu, X., Xiong, X., Zhang, G., Wang, Z., Cheng, C., Wang, X., Bi, X., et al.: Seasonal variations of imidazoles in urban areas of Beijing and Guangzhou, China by single particle mass spectrometry, Science of The Total Environment, 844, 156 995, https://doi.org/10.1016/j.scitotenv.2022.156995, 2022.

Liao, H. and Seinfeld, J. H.: Global impacts of gas-phase chemistry-aerosol interactions on direct radiative forcing by anthropogenic aerosols and ozone, Journal of Geophysical Research: Atmospheres, 110, https://doi.org/10.1029/2005JD005907, 2005.

Liao, Z., Ling, Z., Gao, M., Sun, J., Zhao, W., Ma, P., Quan, J., and Fan, S.: Tropospheric Ozone Variability Over Hong Kong Based on Recent 20 years (2000–2019) Ozonesonde Observation, Journal of Geophysical Research: Atmospheres, 126, e2020JD033 054, https://doi.org/https://doi.org/10.1029/2020JD033054, e2020JD033054 2020JD033054, 2021.

Louie, Peter KK, e. a.: PM2.5 chemical composition in Hong Kong: urban and regional variations, Science of The Total Environment, 338, 267–281, https://doi.org/https://doi.org/10.1016/j.scitotenv.2004.07.021, 2005.

Louie, P. K., Watson, J. G., Chow, J. C., Chen, A., Sin, D. W., and Lau, A. K.: Seasonal characteristics and regional transport of PM2. 5 in Hong Kong, Atmospheric Environment, 39, 1695–1710, https://doi.org/10.1016/j.atmosenv.2004.11.017, 2005.

Ma, L., Guzman, C., Niedek, C., Tran, T., Zhang, Q., and Anastasio, C.: Kinetics and mass yields of aqueous secondary organic aerosol from highly substituted phenols reacting with a triplet excited state, Environmental Science & Technology, 55, 5772–5781, 2021.

Ma, L., Worland, R., Heinlein, L., Guzman, C., Jiang, W., Niedek, C., Bein, K. J., Zhang, Q., and Anastasio, C.: Seasonal variations in photooxidant formation and light absorption in aqueous extracts of ambient particles, EGUsphere, 2023, 1–31, https://doi.org/10.5194/egusphere-2023-861, 2023a.

Ma, L., Worland, R., Jiang, W., Niedek, C., Guzman, C., Bein, K. J., Zhang, Q., and Anastasio, C.: Predicting photooxidant concentrations in aerosol liquid water based on laboratory extracts of ambient particles, EGUsphere, 2023, 1–36, https://doi.org/10.5194/egusphere-2023-566, 2023b.

Ma, L., Worland, R., Tran, T., and Anastasio, C.: Evaluation of Probes to Measure Oxidizing Organic Triplet Excited States in Aerosol Liquid Water, Environmental Science & Technology, https://doi.org/10.1021/acs.est.2c09672, 2023c.

Mabato, B. R. G., Lyu, Y., Ji, Y., Li, Y. J., Huang, D. D., Li, X., Nah, T., Lam, C. H., and Chan, C. K.: Aqueous secondary organic aerosol formation from the direct photosensitized oxidation of vanillin in the absence and presence of ammonium nitrate, Atmospheric Chemistry and Physics, 22, 273–293, https://doi.org/10.5194/acp-22-273-2022, 2022.

Mabato, B. R. G., Li, Y. J., Huang, D. D., Wang, Y., and Chan, C. K.: Comparison of aqueous secondary organic aerosol (aqSOA) product distributions from guaiacol oxidation by non-phenolic and phenolic methoxybenzaldehydes as photosensitizers in the absence and presence of ammonium nitrate, Atmospheric Chemistry and Physics, 23, 2859–2875, https://doi.org/10.5194/acp-23-2859-2023, 2023.

Maizel, A. C. and Remucal, C. K.: The effect of probe choice and solution conditions on the apparent photoreactivity of dissolved organic matter, Environmental Science: Processes & Impacts, 19, 1040–1050, 2017.

Manfrin, A., Nizkorodov, S. A., Malecha, K. T., Getzinger, G. J., McNeill, K., and Borduas-Dedekind, N.: Reactive oxygen species production from secondary organic aerosols: the importance of singlet oxygen, Environmental Science & Technology, 53, 8553–8562, https://doi.org/10.1021/acs.est.9b01609, 2019.

McCabe, A. J. and Arnold, W. A.: Reactivity of triplet excited states of dissolved natural organic matter in stormflow from mixed-use watersheds, Environmental Science & Technology, 51, 9718–9728, https://doi.org/10.1021/acs.est.7b01914, 2017.

McNeill, K. and Canonica, S.: Triplet state dissolved organic matter in aquatic photochemistry: reaction mechanisms, substrate scope, and photophysical properties, Environmental Science: Processes & Impacts, 18, 1381–1399, https://doi.org/10.1039/C6EM00408C, 2016.

Nah, T. and Lam, Y. H.: Influence of urban heat islands on seasonal aerosol acidity and aerosol liquid water content in humid subtropical Hong Kong, South China, Atmospheric Environment, 289, 119 321, https://doi.org/https://doi.org/10.1016/j.atmosenv.2022.119321, 2022.

Nah, T., Lam, Y. H., Yang, J., and Yang, L.: Long-term trends and sensitivities of PM2.5 pH and aerosol liquid water to chemical composition changes and meteorological parameters in Hong Kong, South China: Insights from 10-year records from three urban sites, Atmospheric Environment, 302, 119 725, https://doi.org/https://doi.org/10.1016/j.atmosenv.2023.119725, 2023.

Nguyen, T. K. V., Zhang, Q., Jimenez, J. L., Pike, M., and Carlton, A. G.: Liquid water: Ubiquitous contributor to aerosol mass, Environmental Science & Technology Letters, 3, 257–263, https://doi.org/10.1021/acs.estlett.6b00167, 2016.

770   Nolte, T. M. and Peijnenburg, W. J.: Aqueous-phase photooxygenation of enes, amines, sulfides and polycyclic aromatics by singlet (a1Δg) oxygen: prediction of rate constants using orbital energies, substituent factors and quantitative structure–property relationships, Environmental Chemistry, 14, 442–450, https://doi.org/10.1071/EN17155, 2018.

Ossola, R., Jönsson, O. M., Moor, K., and McNeill, K.: Singlet oxygen quantum yields in environmental waters, Chemical Reviews, 121, 4100–4146, 2021.

775   Pathak, R. K., Yao, X., Lau, A. K., and Chan, C. K.: Acidity and concentrations of ionic species of PM2. 5 in Hong Kong, Atmospheric Environment, 37, 1113–1124, https://doi.org/10.1016/S1352-2310(02)00958-5, 2003.

Powelson, M. H., Espelien, B. M., Hawkins, L. N., Galloway, M. M., and De Haan, D. O.: Brown Carbon Formation by Aqueous-Phase Carbonyl Compound Reactions with Amines and Ammonium Sulfate, Environmental Science & Technology, 48, 985–993, https://doi.org/10.1021/es4038325, pMID: 24351110, 2014.

780   Rounds, S. A., Wilde, F. D., and Ritz, G. F.: Chapter A6. Section 6.2. Dissolved oxygen, Tech. rep., US Geological Survey, 2006.

Seinfeld, J. H. and Pandis, S. N.: Atmospheric chemistry and physics: from air pollution to climate change, John Wiley & Sons, 2016.

Tanner, P. A. and Law, P.-T.: Effects of synoptic weather systems upon the air quality in an Asian megacity, Water, Air, and Soil Pollution, 136, 105–124, https://doi.org/10.1023/A:1015275404592, 2002.

Tratnyek, P. G. and Hoigne, J.: Oxidation of substituted phenols in the environment: a QSAR analysis of rate constants for reaction with 785   singlet oxygen, Environmental science & technology, 25, 1596–1604, https://doi.org/10.1021/es00021a011, 1991.

Tsentalovich, Y. P., Lopez, J., Hore, P., and Sagdeev, R.: Mechanisms of reactions of flavin mononucleotide triplet with aromatic amino acids, Spectrochimica Acta Part A: Molecular and Biomolecular Spectroscopy, 58, 2043–2050, https://doi.org/10.1016/S1386-1425(01)00652-7, 2002.

Walling, C. and Gibian, M. J.: Hydrogen Abstraction Reactions by the Triplet States of Ketones1, Journal of the American Chemical Society, 790   87, 3361–3364, https://doi.org/10.1021/ja01093a014, 1965.

Wang, Q., Zhou, Y., Ma, N., Zhu, Y., Zhao, X., Zhu, S., Tao, J., Hong, J., Wu, W., Cheng, Y., and Su, H.: Review of Brown Carbon Aerosols in China: Pollution Level, Optical Properties, and Emissions, Journal of Geophysical Research: Atmospheres, 127, e2021JD035 473, https://doi.org/https://doi.org/10.1029/2021JD035473, e2021JD035473 2021JD035473, 2022.

Weishaar, J. L., Aiken, G. R., Bergamaschi, B. A., Fram, M. S., Fujii, R., and Mopper, K.: Evaluation of specific ultraviolet absorbance as an 795   indicator of the chemical composition and reactivity of dissolved organic carbon, Environmental science & technology, 37, 4702–4708, https://doi.org/10.1021/es030360x, 2003.

Wilkinson, F., Helman, W. P., and Ross, A. B.: Quantum yields for the photosensitized formation of the lowest electronically excited singlet state of molecular oxygen in solution, Journal of physical and chemical reference data, 22, 113–262, 1993.

Wong, Y. K., Huang, X., Louie, P. K., Yu, A. L., Chan, D. H., and Yu, J. Z.: Tracking separate contributions of diesel and gasoline vehicles 800   to roadside PM 2.5 through online monitoring of volatile organic compounds and PM 2.5 organic and elemental carbon: a 6-year study in Hong Kong, Atmospheric Chemistry and Physics, 20, 9871–9882, https://doi.org/10.5194/acp-20-9871-2020, 2020.

Yang, J., Ma, L., He, X., Au, W. C., Miao, Y., Wang, W.-X., and Nah, T.: Measurement report: Abundance and fractional solubilities of aerosol metals in urban Hong Kong – insights into factors that control aerosol metal dissolution in an urban site in South China, Atmospheric Chemistry and Physics, 23, 1403–1419, https://doi.org/10.5194/acp-23-1403-2023, 2023.

805   Yihui, D. and Chan, J. C.: The East Asian summer monsoon: an overview, Meteorology and Atmospheric Physics, 89, 117–142, https://doi.org/10.1007/s00703-005-0125-z, 2005.

Yu, L., Smith, J., Laskin, A., Anastasio, C., Laskin, J., and Zhang, Q.: Chemical characterization of SOA formed from aqueous-phase reactions of phenols with the triplet excited state of carbonyl and hydroxyl radical, Atmospheric Chemistry and Physics, 14, 13 801–13 816, https://doi.org/10.5194/acp-14-13801-2014, 2014.

810 Yuan, J.-F., Huang, X.-F., Cao, L.-M., Cui, J., Zhu, Q., Huang, C.-N., Lan, Z.-J., and He, L.-Y.: Light absorption of brown carbon aerosol in the PRD region of China., Atmospheric Chemistry & Physics Discussions, 15, https://doi.org/10.5194/acp-16-1433-2016, 2015.

Zepp, R. G., Schlotzhauer, P. F., and Sink, R. M.: Photosensitized transformations involving electronic energy transfer in natural waters: role of humic substances, Environmental Science & Technology, 19, 74–81, https://doi.org/10.1021/es00131a008, 1985.

Zhang, X., Yuan, Z., Li, W., Lau, A. K., Yu, J. Z., Fung, J. C., Zheng, J., and Alfred, L.: Eighteen-year trends of local and non-local
815 impacts to ambient PM10 in Hong Kong based on chemical speciation and source apportionment, Atmospheric Research, 214, 1–9, https://doi.org/10.1016/j.atmosres.2018.07.004, 2018.